

Glutamatergic projection neurons in the basal forebrain underlie learned olfactory associational valence assignments

Received: 16 April 2025

Accepted: 4 January 2026

Published online: 16 January 2026

 Check for updates


Pey-Shyuan Chin^{1,2}, Zhuokun Ding^{1,3}, Mikhail Kochukov^{2,4}, Snigdha Srivastava^{2,4,5}, Elizabeth H. Moss⁶, Qingchun Tong^{7,8}   & Benjamin R. Arenkiel^{1,2,4}  

Sensory perception is shaped by experience, giving stimuli behavioral significance. Basal forebrain (BF) cholinergic neurons in mice, which are crucial for arousal and motivation, also regulate sensory processing. Within BF nuclei, glutamatergic (vGlut2^{BF}) neurons receive cholinergic input and modulate behaviors, but their roles in encoding sensory significance remain unclear. Using *in vivo* calcium imaging, we found that vGlut2^{BF} neurons initially poorly encoded odor identity. However, their response to conditioned odors increased following associative learning, and their population activity more distinctly encoded paired stimuli, reflecting emergent value representation. Furthermore, pairing stimulation or inhibition of vGlut2^{BF} neurons with specific odors altered odor preferences, suggesting that appropriately timed vGlut2^{BF} neuronal activity is sufficient to influence valence assignment. Our findings reveal that vGlut2^{BF} neurons transform sensory input into motivationally significant stimuli, positioning the BF as a key hub for linking sensory processing with motivational states and experience-driven plasticity.

The behavior of organisms is intricately shaped by the neural representations of the external world^{1,2}, where salient sensory stimuli are transformed into value-driven representations that guide action. The basal forebrain (BF) cholinergic system plays a critical role in feedback and feedforward sensory processing^{3–5}. The projections from basal forebrain cholinergic neurons (BFCNs) to the sensory cortex send feedback information to modulate sensory processing, including amplifying signal-to-noise ratios of cortical activity to enhance the detection of sensory input^{6–12}. Receiving inputs from multiple sensory-related areas and cortical regions involved in regulating cognition^{13–16}, the BF is an ideal region for investigating how sensory information is represented naturally and shaped through associative learning. BFCNs

are activated by both positive and negative valence stimuli^{17–20} and play a significant role in associative learning by exhibiting distinct neuronal responses to cues associated with reward and/or punishment^{17,21–23}. While BFCNs are the most extensively studied neuronal population in the BF³, the BF comprises diverse neuronal types, including both GABAergic and glutamatergic projection neuron populations^{24,25}. These different types of projection neurons extend to diverse brain areas, form reciprocal connections, and receive direct fast cholinergic neurotransmission from BFCNs^{14,26–30}. As such, these non-cholinergic populations have been shown to participate in adaptive circuits that transform novel sensory stimuli into meaningful representations. For example, it has been previously shown that non-cholinergic

¹Department of Neuroscience, Baylor College of Medicine, Houston, TX, USA. ²Jan and Dan Duncan Neurological Research Institute, Texas Children's Hospital, Houston, TX, USA. ³Department of Ophthalmology, Byers Eye Institute, Stanford University School of Medicine, Stanford, CA, USA. ⁴Department of Molecular and Human Genetics, Baylor College of Medicine, Houston, TX, USA. ⁵Medical Scientist Training Program, Baylor College of Medicine, Houston, TX, USA. ⁶Department of Anesthesiology and Perioperative Medicine, Oregon Health & Science University, Portland, OR, USA. ⁷Brown Institute of Molecular Medicine at McGovern Medical School, University of Texas Health Science Center of Houston, Houston, TX, USA. ⁸Neuroscience Program of UTHealth Houston & MD Anderson Cancer Center Graduate School of Biomedical Sciences, University of Texas Health Science Center of Houston, Houston, TX, USA.

 e-mail: Qingchun.Tong@uth.tmc.edu; arenkiel@bcm.edu

populations within the BF encode motivational salience, predict stimuli associated with behavioral performance, and contribute to olfactory associative learning^{17,31–33}. However, the roles of specific non-cholinergic subtypes in encoding motivationally significant sensory stimuli and whether/how their neural activity correlates with motivation-driven behaviors is not well understood.

Glutamatergic BF neurons (vGlut2^{BF}) are of particular interest because they are excited via fast cholinergic transmission and project out of their respective nuclei to numerous downstream targets involved in diverse behaviors^{34–36}. Notably, we and others have found that BFCN-targeted vGlut2^{BF} neurons within the Diagonal Band of Broca are responsive to both appetitive and aversive external stimuli^{34–37}, and over-activation of these neurons induces an overriding hypophagic state, altering the perception of rewarding food^{34,38}. vGlut2^{BF} neurons make functional connections with regions that include the lateral hypothalamus (LH), lateral habenula (LHb), and the ventral tegmental area (VTA), which are crucial for guiding feeding, avoidance, and other reward/punishment-related behaviors^{34–37,39–41}. Thus, whether in conjunction or directly downstream of cholinergic transmission, this subcortical processing via vGlut2^{BF} neurons may act as a neural shortcut, bypassing more complex cortical centers and rapidly eliciting physiologically important behaviors. These data suggest that vGlut2^{BF} neurons are critical for processing different sensory information and driving subsequent motivational behaviors. However, how vGlut2^{BF} projection neurons represent sensory information with different values, and how their activity is involved in motivational behaviors such as associative learning and valence assignment, remains unclear.

To address this, we focused on olfaction, as the basal forebrain receives strong inputs from all major olfactory processing regions^{13,42}. Although often regarded as a monolithic structure, the basal forebrain is composed of discrete regions with distinct patterns of afferent and efferent connectivity^{15,43,44}. Basal forebrain cholinergic neurons exhibit region-specific response patterns; for instance, neurons in caudal regions such as the globus pallidus/substantia innominata (GP/Sl) and in rostral regions such as the horizontal limb of the diagonal band (HDB) differentially process sensory, reward, and aversion-related stimuli¹⁹. Here, we targeted the horizontal limb of the diagonal band (HDB) in the basal forebrain, where it not only receives olfactory information but also sends projections to the olfactory bulb and modulates olfactory perception^{45–47}. Also, lesioning, external stimulation of the HDB, or silencing specific neuronal populations within it has been shown to affect olfactory-mediated behaviors^{5,33,48,49}. In this study, we used *in vivo* calcium imaging to ask how specific olfactory stimulus features—such as identity and/or associated values—are represented by vGlut2^{BF} neurons. We found that while individual vGlut2^{BF} neurons do not initially distinctly represent specific odor identities, they can decode odors with associated values. Moreover, vGlut2^{BF} neurons show differential response properties with associative learning that involve reward or punishment, suggesting a role in representing motivational salience. Further, we found that direct modulation of vGlut2^{BF} neuronal activity impacts olfactory learning and valence assignment. That is, pairing vGlut2^{BF} neuronal activation with given odors induces avoidance, whereas inhibition induces preference. Taken together, these studies reveal the glutamatergic projection neurons within the basal forebrain as key players in linking sensory stimuli with motivational states and experience-driven plasticity.

Results

vGlut2^{BF} neurons exhibit broad odor responses but do not encode odor identity or innate valence

Since vGlut2^{BF} neurons have previously been shown to be activated by both positive and negative olfactory stimuli^{34–37}, we first examined their baseline response to different types of volatilized odorants. Using

GRIN lens miniscope imaging in head-fixed vGlut2-Cre mice expressing GCaMP8s, we recorded the neuronal activity in the horizontal limb of the diagonal band of Broca (HDB) of the basal forebrain at single-cell resolution during passive odor delivery (Fig. 1A and Supplementary Fig. 1A, B). For this, mice were exposed to four different neutral odors that were not associated with any valence: rose oil, eugenol, methyl salicylate, and anisole. All odors were diluted in mineral oil at a 2% concentration. Each odor was presented for 2 s 10 times in a randomized order with a modified odor delivery system⁵⁰ (Fig. 1B). Using pre-packaged detection algorithms based on principal and independent component analyses (PCA/ICA) and fluorescence response tracking via Inscopix software, individual neurons were first spatially defined, and their calcium dynamics were extracted over time (Fig. 1C, D, Supplementary Video 1).

The responses of individual vGlut2^{BF} neurons before and after odor onset (Fig. 1E; Eugenol and Methyl Salicylate as examples, and Supplementary Fig. 1C) were grouped into categories: excited, inhibited, or non-responsive. More specifically, we defined excited neurons as those that showed elevated activity levels and reached at least three standard deviations higher than their baselines during a 2-second odor presentation period, whereas inhibited neurons were those with activity three standard deviations lower than their respective baselines. On average, each odor recruited 28.5% of all identified neurons to be responsive, with similar distributions of excited, inhibited, and non-responsive cells across different odors (Fig. 1F, Supplementary Fig. 1E, and Supplementary Table 1). Notably, 55.7% of neurons were not excited by any odors (Fig. 1G), and 61.5% of all excited cells showed increased activity to more than one odor, suggesting a lack of specificity for individual odorants (Fig. 1G).

Although individual cell responses appeared to lack odor specificity, we next directly tested if the observed populations were capable of reporting or encoding odor identity at baseline. To this end, we trained logistic regression binary models (see methods) to decode single-trial odor responses using population responses. The model could not decode odors significantly above chance (Fig. 1H), indicating a lack of ability to differentiate odors based on the recorded neuronal response patterns. These data suggest that, at baseline, vGlut2^{BF} neurons do not distinctly represent specific odorants.

As vGlut2^{BF} neurons have previously been identified to drive aversion-like behaviors^{34–36}, we tested whether vGlut2^{BF} neurons preferentially encode innately aversive odors. Using the same imaging approach, we recorded neuronal responses of vGlut2^{BF} neurons to four natural odorants considered to be innately aversive to mice: cadaverine, isopentylamine, butyric acid, and 2-methylbutylamine^{51–53} (Supplementary Fig. 1D). Using the same quantitative approach, we found that the number of responsive neurons and the overall magnitude of responses (AUC during odor presentation) during the 2-second odor presentation period for each of the aversive odors were not different from those observed with neutral odorants (Supplementary Fig. 1F, G). Moreover, the model failed to decode the tested aversive odors above chance (Supplementary Fig. 1H), suggesting that vGlut2^{BF} neurons do not selectively encode odor identity regardless of innate odor valence.

Finally, we asked if vGlut2^{BF} neurons could directly encode the assumed inherent valences of the odors. Toward this, we trained the decoding model to distinguish population responses to neutral odors versus aversive odors, and the accuracy remained near chance (Supplementary Fig. 1I). Together, these results suggest that during initial exposure to neutral or naturally aversive odors, which lack any learned associations, odor identity and/or innate valence are not represented by vGlut2^{BF} neurons.

vGlut2^{BF} neurons alter odor responses following associations

Although vGlut2^{BF} neurons did not encode odor identity or valence at baseline, the basal forebrain is able to integrate sensory information to modulate cortical activity and guide behavior^{13,54}. We therefore next

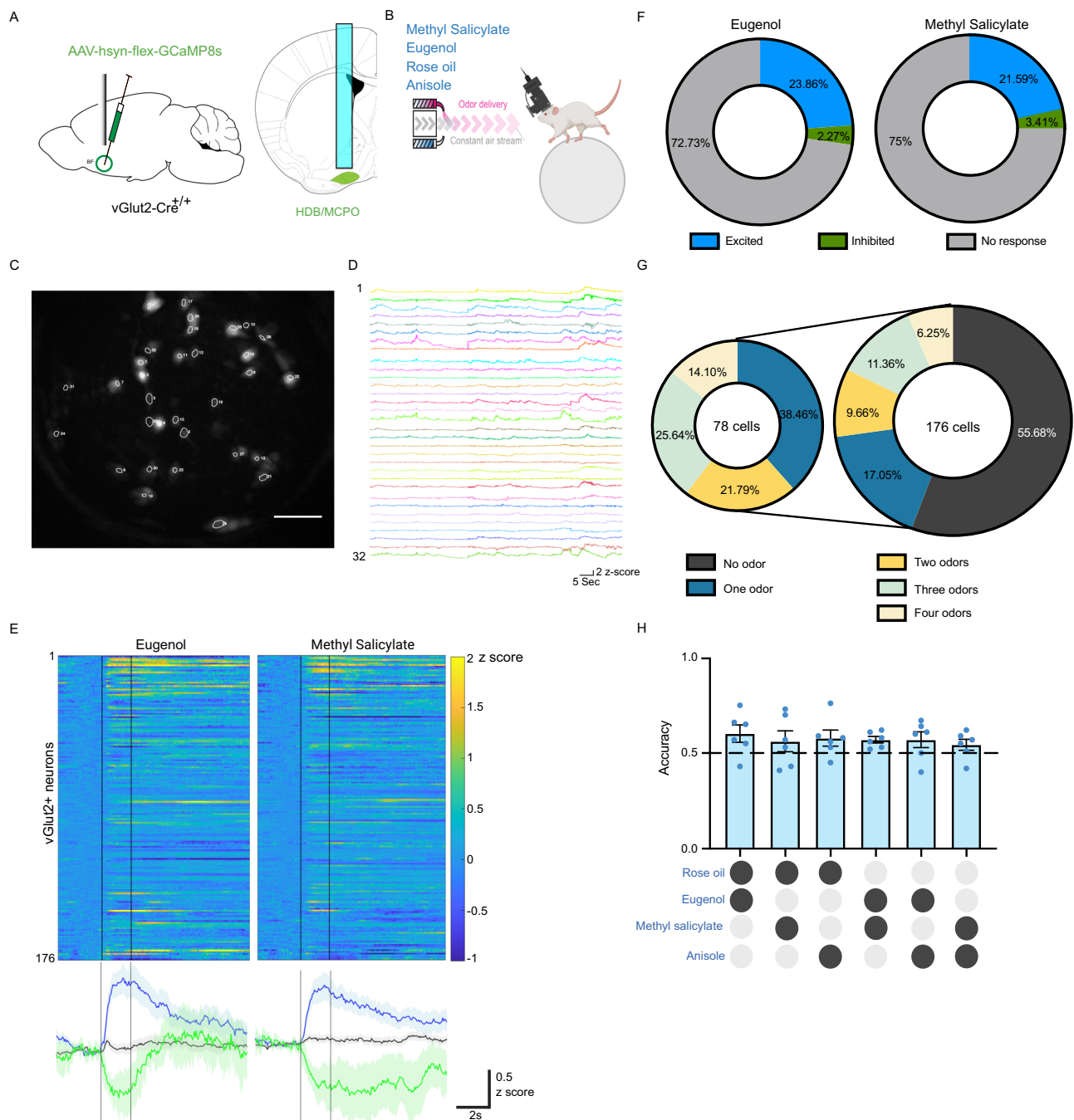
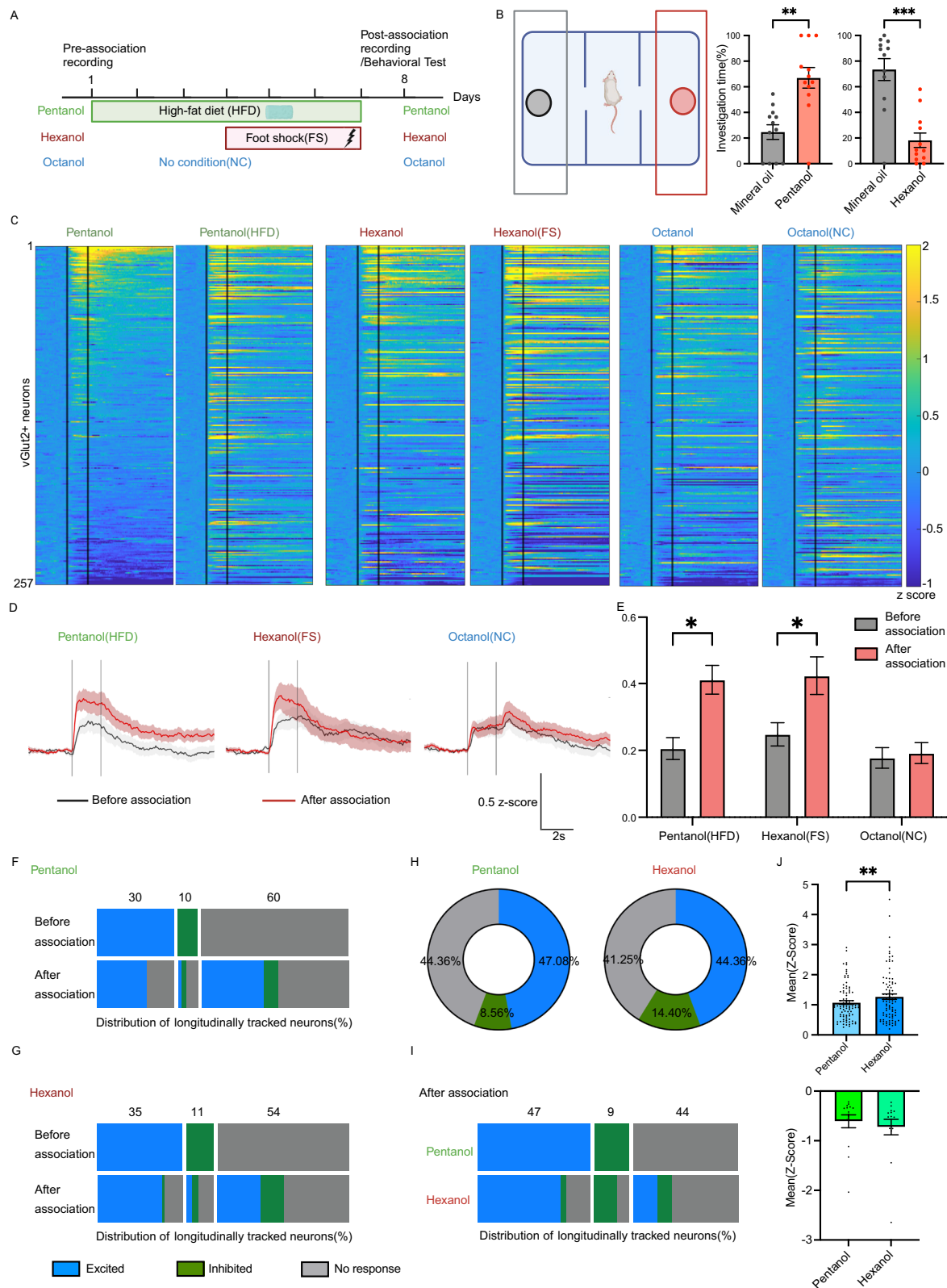


Fig. 1 | vGlut2^{BF} neurons are odor responsive but do not show odor specificity.

A Schematic of GRIN lens implantation above the horizontal limb of the diagonal band (HDB) and Magnocellular Preoptic Nucleus (MCPO) in vGlut2-IRES-Cre mice injected with AAV-hSyn-FLEX-GCaMP8s. **B** Experimental setup for odor screening and in vivo calcium imaging with a Miniscope. **C** Representative field of view showing vGlut2^{BF} neurons through the GRIN lens. Scale bar, 100 μ m. **D** Extracted calcium traces from the 32 neurons shown in (C). **E** Heatmap of odor-evoked responses from all recorded vGlut2^{BF} neurons for two example odors, Eugenol and Methyl Salicylate (MSC). Below each heatmap, population-averaged traces are shown for neurons categorized as excited (blue), non-responsive (black), or inhibited (green). The timescale matches between heatmaps and average traces. Black vertical lines indicate odor onset and offset. **F** Proportion of response types during odor presentation. Left: responses to Eugenol—excited (23.86%), inhibited (2.27%), non-responsive (72.73%). Right: responses to MSC—excited (21.59%), inhibited (3.41%), non-responsive (75%). ($n = 176$ neurons from 6 animals). **G** Distribution of odor tuning across the population. Right: proportion of all

neurons grouped by the number of odors that elicited excitatory responses, including neurons that did not respond to any presented odor ($n = 176$ neurons). Left: distribution restricted to neurons classified as excited ($n = 78$ neurons), grouped by the number of odors they responded to. **H** Decoding accuracy for distinguishing odor pairs among the four tested odors. Accuracy was compared to chance level (0.5) using two-tailed Student's t -tests with Holm-Šidák correction. Black circles indicate the odor pair used for the accuracy comparison. Pairwise comparisons: Rose oil vs. Eugenol ($p = 0.75$), Rose oil vs. MSC ($p = 0.59$), Rose oil vs. Anisole ($p = 0.59$), Eugenol vs. MSC ($p = 0.65$), Eugenol vs. Anisole ($p = 0.57$), MSC vs. Anisole ($p = 0.59$) ($n = 6$ animals). Data are presented as mean \pm s.e.m. Illustration in (B) was created in BioRender. Chin, P. (2025) <https://BioRender.com/74qwul9>. Source data are provided as a Source Data file. Right panel in (A) is reprinted from The Mouse Brain in Stereotaxic Coordinates, 3rd edition, Paxinos G. & Franklin K.B.J., Figures 27, Copyright (2008), with permission from Elsevier.



asked if odor representations change when odors are associated with a salient outcome. Toward this, we paired innocuous/neutral monomolecular odorants with positive or negative reinforcement, and recorded odor-evoked vGluT2^{BF} neuron activity before and after this association. Specifically, we paired Pentanol with a positive stimulus (60% fat, high-fat diet) and Hexanol with a negative stimulus (foot shock), while Octanol served as an unpaired control (Fig. 2A). Since

olfactory responses are also prone to habituation, we also included an additional control odor (Heptanol) with three days of habituation (Supplementary Fig. 2B). To validate the behavioral association of the paired odors, we conducted an odor preference test in a three-chamber spatial choice arena in which the positively or negatively paired odors were tested against mineral oil controls. Consistent with association pairing, mice spent significantly more time in regions with

Fig. 2 | vGlut2^{BF} neuron responses increase after odor association with positive or negative stimuli. **A** Experimental timeline for olfactory conditioning. Pentanol (5%) was paired with high-fat diet (HFD), Hexanol (5%) with foot shock (FS), and Octanol was unpaired. **B** Behavioral preference/avoidance in GRIN lens-implanted mice. Time spent with HFD-associated odor (Pentanol) and the foot-shock-associated odor (Hexanol), compared to time spent with mineral oil (odorless control). The associated odor is shown in red, and the odorless control is shown in gray. $n = 12$ animals; paired two-tailed Student's t -test: Pentanol, $p = 0.0005$; Hexanol, $p < 0.0001$. **C** Heatmaps of vGlut2^{BF} neuronal responses to Pentanol (HFD), Hexanol (FS), and Octanol before and after association. For each odor, the left panel shows pre-association responses, and the right shows post-association responses. Black vertical lines indicate odor onset and offset. **D** Population-average traces of all recorded neurons before (black) and after (red) association for each odor. Black vertical lines indicate odor onset and offset. **E** Quantification of mean odor-evoked responses across neurons before (gray) and after (red) association. $n = 257$ neurons from 12 animals; paired two-tailed Student's t -test: Pentanol, $p < 0.0001$; Hexanol, $p < 0.0001$; Octanol, $p = 0.2483$. Classification of neuronal responses to Pentanol

(**F**) and Hexanol (**G**) before and after association. Neuronal responses after association were grouped based on their pre-association state (excited (blue), inhibited (green), or non-responsive (gray)). Percentages indicate the distribution of response types before association. **H** Proportion of excitatory, inhibitory, and non-responsive neurons after association for Pentanol and Hexanol. Pentanol: excited (47.08%), inhibited (8.56%), no response (44.36%). Hexanol: excited (44.36%), inhibited (14.40%), no response (41.25%). **I** Hexanol-evoked responses grouped by each neuron's response category to Pentanol after association. Percentages indicate the distribution of excited, inhibited, and non-responsive for Pentanol. **J** Mean z-scored responses during the 2-s odor period for neurons excited (top) or inhibited (bottom) by both HFD- and FS-associated odors. Paired two-tailed Student's t -test: excited neurons ($n = 88$ neurons), $p = 0.0046$; inhibited neurons ($n = 15$ neurons), $p = 0.1067$. Data are presented as mean \pm s.e.m. * $P < 0.05$, ** $P < 0.01$, *** $P < 0.001$, **** $P < 0.0001$. Illustrations in (**A**) were Created in BioRender. Chin, P. (2025) <https://BioRender.com/74qwul9>. Source data are provided as a Source Data file.

high-fat diet-associated odors than the control odor, and less time in regions with foot shock-paired odors (Fig. 2B). These behavioral data confirm that the association paradigm was capable of effectively establishing and/or assigning valence to the associated odors, providing an experimental framework to investigate how the basal forebrain circuitry is involved in this process.

Following association, vGlut2^{BF} neurons exhibited increased responses to both positive (high-fat diet) and negative associations (foot shock), while responses to the unpaired control and the habituated odor remained unchanged (Fig. 2C–E; Supplementary Fig. 2B–E). Both the newly recruited neurons and the neurons that were excited before and after association (stable neurons) increased their activity after association (Supplementary Fig. 2A). These data show that both the stable and newly recruited neurons contribute to activity changes following association. To quantify patterns of change in the response properties of individual cells, we examined how previously non-responsive neurons were recruited. Among the recorded cells that were excitable pre-association, the majority remained excited after association (66.23% for Pentanol (high-fat diet); 75.56% for Hexanol (foot shock)). However, a significant fraction of previously non-responsive neurons became excited after association in response to both positive and negative association (42.20% recruited for Pentanol; 31.65% recruited for Hexanol) (Fig. 2F, G, and Supplementary Table 2). These data indicate that vGlut2^{BF} neurons alter their responses with conditioned and/or learned positive and negative values. A fraction of non-responsive neurons became excited after habituation (15.88%), but not as much as the percentage followed by reinforcement association (Supplementary Fig. 2F and Supplementary Table 2).

As the response properties changed following learned association, we also examined if vGlut2^{BF} neurons were capable of encoding learned positive and/or negative associations. We found that most vGlut2^{BF} neurons (72.72%) that were excited by positive-conditioned odors also responded to the negative-conditioned odor. However, a subset of neurons showed selectivity for either positive or negative associations. For example, 21.5% of neurons excited by Pentanol responded exclusively to Pentanol, while 23.7% neurons excited by Hexanol responded exclusively to Hexanol (Fig. 2H, I, and Supplementary Table 2). Thus, most responsive cells encode both associations, while only subgroups of neurons that encode specific valence may exist. Notably, neurons activated by both associations exhibited significantly stronger responses to the negative odor (Fig. 2J). Given that locomotor speed correlates with acetylcholine release⁵⁵, an indicator of cholinergic neuronal activity and arousal state, we also analyzed their locomotion on the head-fixed wheel following odor presentations before and after association. We found that locomotion during negative odor presentations increased compared to pre-association, whereas responses to positive odors remained unchanged

(Supplementary Fig. 2I, J), suggesting a difference in arousal levels to odors with distinct associations.

Together, these findings demonstrate that vGlut2^{BF} neurons do not encode odor identity or innate valence at baseline but adaptively alter their responses following associative learning, particularly for odors with motivational significance.

Associative learning reshapes population-level odor representations

As we observed an increase in single-cell response levels and recruitment of more cells following stimulus-paired odor associations, we next examined how such associations influence population-level neural dynamics. Toward this, we applied principal components analysis (PCA) to analyze the trial-averaged trajectories of vGlut2^{BF} population activity. We included responses from baseline (three seconds preceding odor onset) to ten seconds following odor onset. We plotted the trajectories of neural responses to the high-fat diet-associated odor (Pentanol) and the control odor (Octanol) on one PCA map, and the foot shock-associated odor (Hexanol) and the control odor (Octanol) on another PCA map (Fig. 3A–C). These visualizations revealed a clear separation between the post-association odor trajectories and both the pre-association and control odor trajectories. To quantify the proximity between odor-evoked trajectories—which reflects the similarity of neural population responses—we computed the Euclidean distance between trial-averaged activity vectors in high-dimensional cell space. We z-scored calcium responses and averaged them across trials to generate a population activity vector for each odor condition. We then calculated the Euclidean distance (see Methods for the formula) between vectors before and after conditioning to assess how population representations changed with learning. Distances were plotted from baseline (three seconds before odor onset) to 10 s after odor onset (Fig. 3D).

Notably, the Euclidean distance during the odor presentation period between pre- and post-association trajectories was significantly higher for the foot shock-conditioned odor compared to the control odor octanol (Fig. 3D), indicating that aversive conditioning substantially shifted population responses. The Euclidean distance for Heptanol between before and after habituation was not significantly changed compared to Octanol (Supplementary Fig. 2G, H). Finally, we compared the Euclidean distance between Pentanol and Hexanol before and after association. Although this comparison did not reach statistical significance, the distance trended higher after conditioning (Fig. 3E).

Building upon this, we next examined whether these altered neural dynamics enhanced odor decoding accuracy. Towards this, we trained a linear decoder on population responses to the positive conditioned, negative conditioned, habituated, and unpaired odors

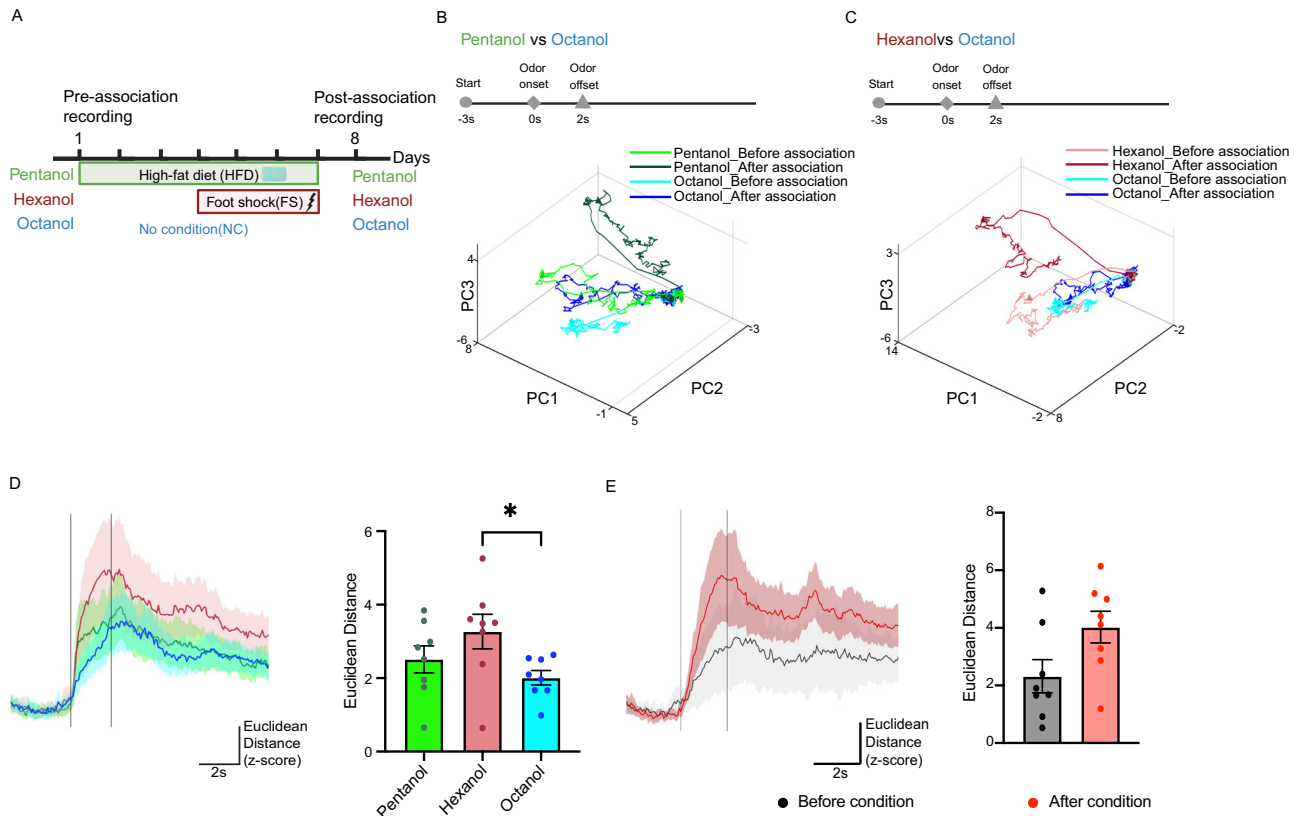


Fig. 3 | PCA trajectories show population response differences after paired-odor association. **A** Experimental paradigm for the association experiments. Pentanol (green) was paired with high-fat diet (positive stimulus) for seven days, Hexanol (red) was paired with foot shock (negative stimulus) for three days, and Octanol (blue) was not associated with any stimulus. Principal component trajectories for odor-evoked population activity before and after association. Circles denote the start of the trajectory, diamonds indicate odor onset, and triangles indicate odor offset. Data are collected from 154 neurons across 8 animals. **B** Trajectories for Pentanol (HFD-associated) and Octanol (unpaired). **C** Trajectories for Hexanol (FS-associated) and Octanol. Light green: Pentanol before association; dark green: Pentanol after association. Light red: Hexanol before association; dark red: Hexanol after association. Light blue: first Octanol exposure; dark blue: second

Octanol exposure. (Color scheme as in (A)). **D** Left: Euclidean distance between trajectories before and after association across time for Pentanol (green), Hexanol (red), and Octanol (blue). Black vertical lines indicate odor onset and offset. Right: Quantification of Euclidean distance during the 2-second odor presentation window ($n = 8$ animals). Paired two-tailed Student's t -tests: Pentanol vs. Octanol, $p = 0.2152$; Hexanol vs. Octanol, $p = 0.0177$. **E** Left: Euclidean distance between Pentanol and Hexanol trajectories before and after association across all time points. Gray: before association; red: after association. Right: Quantification during the 2-second odor period ($n = 8$ animals). Paired two-tailed Student's t -test: $p = 0.053$. Black vertical lines indicate odor onset and offset. Data are presented as mean \pm s.e.m. * $P < 0.05$. Illustration in (A) was Created in BioRender. Chin, P. (2025) <https://BioRender.com/74qwul9>. Source data are provided as a Source Data file.

during a 2-second presentation window (Fig. 4A). We found that decoding accuracy explicitly improved for the conditioned odors following both positive and negative associations (Fig. 4B, C). Specifically, the binary model achieved significantly higher accuracy in distinguishing between the two oppositely conditioned odors (Fig. 4D), while decoding accuracy did not improve when distinguishing between the habituated and the unpaired odor (Fig. 4E), indicating that the altered neural dynamics following association encode distinct association states. Furthermore, the binary model more reliably differentiated conditioned odors from the habituated and the unpaired odors post-association (Fig. 4F, G).

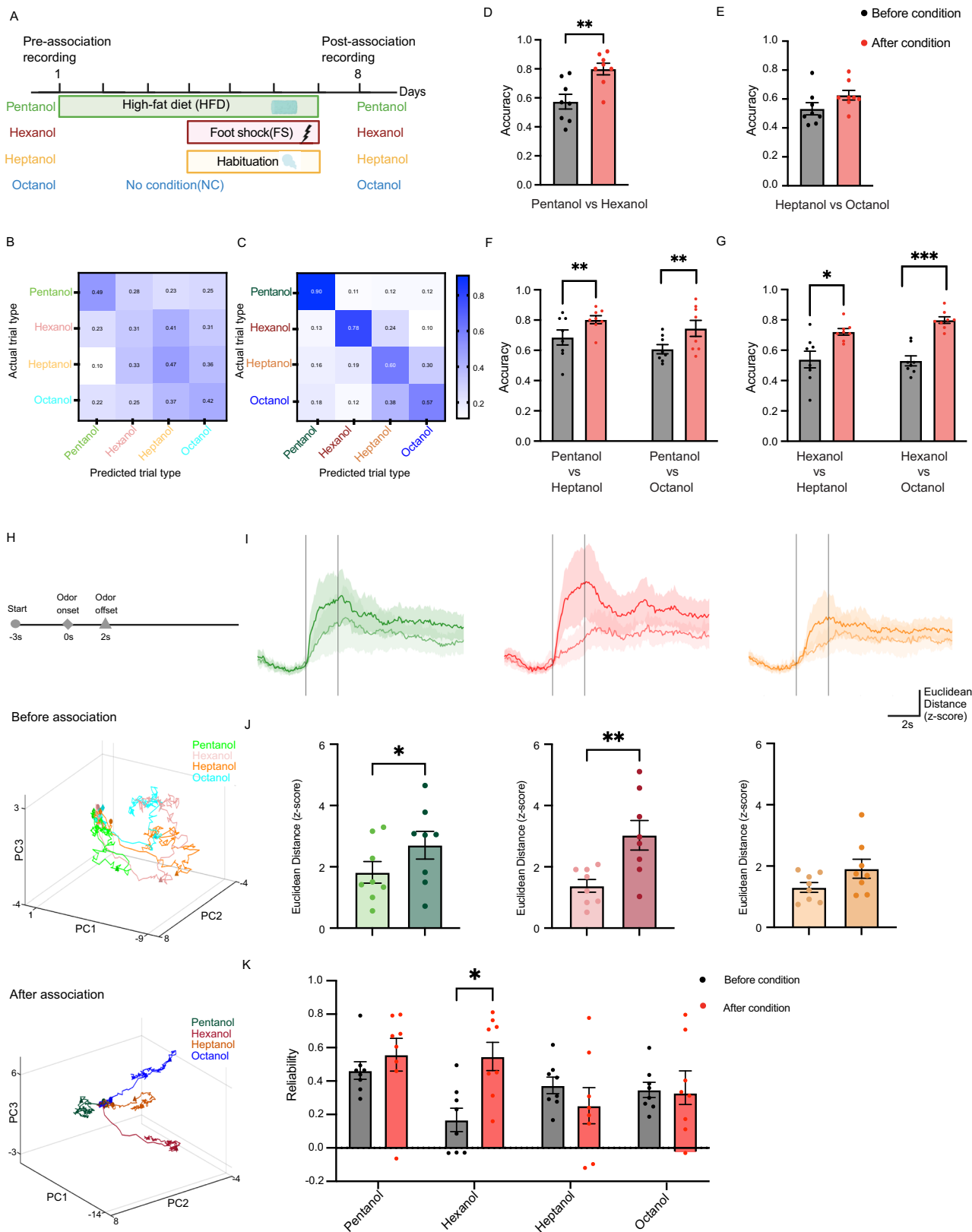
To further explore these dynamics, we plotted conditioned and unconditioned odor response trajectories on a single PCA map. Initially, all odor trajectories displayed spatial proximity (Fig. 4H, top). However, following association, we observed a distinct separation in the response trajectories for conditioned odors, revealing a significant shift in the overall neural representation for the associated odors in high-dimensional population space (Fig. 4H, bottom). We quantified this shift using the Euclidean distance from the unpaired odor (Octanol) as a reference, revealing that the conditioned odors (both Pentanol and Hexanol) deviated significantly from the Octanol post-association. In contrast, the distance between the habituated and the unpaired odor (Heptanol and Octanol) remained unchanged (Fig. 4I, J).

This increase in the Euclidean distance compared to the control odor reflects greater remodeling of the neural code for the associated odors, consistent with changes in odor-associated meaning and salience. We also reasoned that this population-level shift likely drives the model's improved classification accuracy.

Lastly, we examined trial-to-trial response reliability, which could influence decoding accuracy. Our data showed increased trial reliability specifically for negatively associated odors, but not for the positively associated or control odors (Fig. 4K). Together, these results indicate that associative learning alters population responses, enhancing the encoding of odors with associated and/or learned salience.

vGlut2^{BF} neurons contribute to odor-associative learning

Given that associative learning altered the response dynamics of vGlut2^{BF} neurons, we next investigated if these neurons impact odor-associative learning. Toward this, we stereotaxically injected adult vGlut2-Cre mice with conditional AAVs encoding either the inhibitory DREADD receptor hM4Di (Gi-coupled human muscarinic M4 designer receptor exclusively activated by a designer drug) or an mRuby fluorescent control. Specifically, we used AAV-Ef1a-flex-hM4Di-mCherry and AAV-Ef1a-flex-mRuby vectors, delivering them bilaterally into the HDB of vGlut2-Cre mice for conditional expression in vGlut2^{BF} neurons (Fig. 5A–C, Supplementary Fig. 4A). As a validation control, we



performed whole-cell recordings in acute brain slices following the introduction of clozapine-N-oxide (CNO). All recorded hM4Di expressing vGlut2^{BF} neurons (n = 7 cells) showed hyperpolarization to CNO (Fig. 5D), but variable changes in firing behavior. While 2 cells out of 7 showed cessation of spontaneous firing, 3 other cells changed the firing pattern into more burst-like patterns. The latter could possibly

be due to the hyperpolarization-activated HCN channel cationic current, which was previously described in glutamatergic BF neurons⁵⁶. However, this would need to be further confirmed experimentally.

To assess learning behavior while manipulating vGlut2^{BF} neuron activity, we first trained mice expressing either DREADDs or mRuby on an olfactory Go/No-Go task⁵⁷ after a 3-week post-surgery recovery

Fig. 4 | Odor decoding accuracy of vGlut2^{BF} neurons improves following positive and negative associations. **A** Experimental paradigm. Pentanol (green) was paired with HFD (positive stimulus) for seven days. Hexanol (red) was paired with foot shock (negative stimulus) for three days. Heptanol (orange) was presented without reinforcement for three days as a habituation control. Octanol (blue) was not paired with any stimulus. Confusion matrices illustrating decoding of odor identity before **B** and after **C** association. **D** Decoding accuracy for distinguishing Pentanol (HFD-associated) versus Hexanol (FS-associated). Paired two-tailed Student's *t*-test: $p = 0.0056$ ($n = 8$ animals, 154 neurons). **E** Accuracy of decoding two control odors (Heptanol vs. Octanol). Paired two-tailed Student's *t*-test: $p = 0.2364$ ($n = 8$ animals, 154 neurons). **F** Accuracy of decoding Pentanol versus control odors. Paired two-tailed Student's *t*-tests: Pentanol vs. Heptanol, $p = 0.0324$; Pentanol vs. Octanol, $p = 0.0003$ ($n = 8$ animals, 154 neurons). **G** Accuracy of decoding Hexanol versus control odors. Paired two-tailed Student's *t*-tests: Hexanol vs. Heptanol, $p = 0.0055$; Hexanol vs. Octanol, $p < 0.0001$ ($n = 8$ animals, 154 neurons).

H Population response trajectories for the four odors before (top) and after (bottom) association. Circles denote trajectory start; diamonds indicate odor onset; triangles indicate odor offset. Colors follow the scheme in (A). ($n = 8$ animals, 154 neurons). **I** Euclidean distance between Octanol and each of the three other odors—Pentanol (green), Hexanol (red), and Heptanol (orange)—across time. Lighter and darker shades indicate before and after association, respectively. Black vertical lines indicate odor onset and offset. ($n = 8$ animals, 154 neurons). **J** Quantification of Euclidean distances during odor presentation. Paired two-tailed Student's *t*-tests: Pentanol vs. Octanol, $p = 0.0179$; Hexanol vs. Octanol, $p = 0.0061$; Heptanol vs. Octanol, $p = 0.1215$. ($n = 8$ animals, 154 neurons). **K** Trial reliability is computed as the correlation of neuronal response vectors across trials. Paired two-tailed Student's *t*-tests (Before vs. After): Pentanol, $p = 0.4353$; Hexanol, $p = 0.0103$; Heptanol, $p = 0.3922$; Octanol, $p = 0.9595$ ($n = 8$ animals). Data are presented as mean \pm s.e.m. * $P < 0.05$, ** $P < 0.01$. Illustration in (A) was Created in BioRender. Chin, P. (2025) <https://BioRender.com/74qwul9>. Source data are provided as a Source Data file.

period (Fig. 5E). Notably, all mice successfully passed the training stages and moved on to the testing phase. During the training phase, there was no difference in learning ability between the hM4Di and the mRuby injected mice (Supplementary Fig. 3A–C). The mice were then tested on their ability to differentiate between an S+ odor, associated with water as a reward, and an S- odor, indicating no reward availability (Fig. 5E). During this testing phase, each group received an intraperitoneal injection of either CNO (3.5 mg/kg) or saline 30 min before testing. Behavioral performance was quantified using the D prime (d') metric, where higher d' values indicate greater accuracy in distinguishing between the S+ and S- odors, and a zero value represents chance performance⁵⁸. We found that CNO-treated DREADD-expressing mice exhibited a slower learning rate compared to their saline-treated condition or the CNO-treated mRuby-expressing control mice (Fig. 5F, Supplementary Fig. 3D). That is, when vGlut2^{BF} neurons were silenced, although the mice were able to reach the learning criterion, defined as accuracy greater than 85%, they required significantly more blocks to learn to successfully discriminate the S+ vs. S- odors (Fig. 5G). Furthermore, inhibition of vGlut2^{BF} neurons also led to a reduced overall performance, which is shown with the reduced D prime value for the task (Fig. 5H). These data suggest that vGlut2^{BF} neurons are required for associative learning in this Go/No-Go discrimination task.

Given that reduced D prime measures suggested the impaired ability to discriminate associated odors, we next evaluated if vGlut2^{BF} neurons were necessary for odor discrimination independent of learning. Toward this, we performed a habituation/dishabituation task while chemogenetically inhibiting vGlut2^{BF} neurons (Supplementary Fig. 3E). DREADD-expressing and control mice preferred new odors after CNO or saline treatment, suggesting that vGlut2^{BF} inhibition does not impair basic odor detection or discrimination (Supplementary Fig. 3F). Importantly, all mice tested exhibited successful habituation to the first odor (Supplementary Fig. 3G). Overall, these findings suggest that while vGlut2^{BF} neurons are necessary for learning in an odor-discrimination task, they do not affect the fundamental ability to detect or distinguish odors.

Activation or inhibition of vGlut2^{BF} neurons alters odor preference

Prior studies have shown that over-activating vGlut2^{BF} neurons induced an aversive state and reduced food intake^{34–36}. Building upon these findings, we next investigated whether targeted overactivation of vGlut2^{BF} neurons could associate an aversive state to a neutral odor stimulus and/or subsequently alter odor preference. To test this, we utilized Channelrhodopsin-2 (ChR2)-based in vivo optogenetics to selectively and acutely activate vGlut2^{BF} neurons while presenting paired odors. First, we evaluated effective cell type-specific targeting and activation of these cells by injecting AAV-Ef1a-flex-ChR2-EYFP into the HDB of vGlut2-Cre mice (Fig. 6A, left). After allowing

14 days for expression, we confirmed the presence of light-evoked depolarization and action potentials at 20 Hz in brain slices, consistent with our previous findings³⁴ (Fig. 6A, top right).

After verifying ChR2 functionality, we bilaterally delivered the AAV-Ef1a-flex-ChR2-EYFP virus and implanted fiber optics in the HDB of vGlut2-Cre mice (Fig. 6B left, Supplementary Fig. 4B). After recovery, real-time place avoidance assays indicated that mice actively avoided areas associated with the photostimulation of vGlut2^{BF} neurons (Supplementary Fig. 5A, B), suggesting that over-activating these neurons induced an aversive effect. To assess whether this cell type-specific avoidance behavior could be transferred to an odor stimulus, we paired a previously unassociated odor (5% Hexanol) with 2 s of ChR2-mediated vGlut2^{BF} neuron activation in head-fixed mice ($\lambda = 473$ nm, 0.5 Hz, 10 ms pulses, for 10 min per session, five sessions per day for 3 days) (Fig. 6C). Notably, post-pairing, ChR2-expressing mice showed a decrease in the preference index for the zones with the photostimulation-paired odor compared to initial unpaired exposure (Fig. 6D, E, Supplementary Fig. 5C), suggesting an induced odor aversion.

We next investigated whether inhibition of vGlut2^{BF} neurons could drive a positive effect. Toward this, we use the improved chloride-conducting Channelrhodopsin (iChloc) actuator for inhibitory in vivo optogenetics^{59,60}. We injected AAV-Ef1a-flex-iChloc bilaterally into the HDB of vGlut2-Cre mice (Fig. 6A, left). To confirm the inhibitory effect of iChloc on vGlut2^{BF} neurons, we again performed whole-cell current clamp electrophysiology recordings from iChloc-expressing vGlut2^{BF} neurons. With stimulation, we observed a shift in voltage with a concomitant decrease in firing frequency and amplitude due to apparent shunting inhibition in iChloc-expressing neurons (Fig. 6A, bottom right).

Following validation, we injected AAV-Ef1a-flex-iChloc and implanted fiber optics in the HDB of vGlut2-Cre mice and performed real-time place preference (Fig. 6B right, Supplementary Fig. 4B). Mice expressing iChloc spent more time in the area associated with neuronal inhibition (Supplementary Fig. 5A, B), suggesting that vGlut2^{BF} inhibition induced a positive effect. We then paired odor delivery (2 s of 5% Pentanol) with inhibition of vGlut2^{BF} neurons using iChloc ($\lambda = 473$ nm, 0.5 Hz, 10 ms pulses, for 10 min per session, five sessions per day) concurrently over three days (Fig. 6C). Post-pairing, iChloc-expressing mice showed an increase in preference index in zones with the paired odor compared to periods before pairing, suggesting a light-induced odor preference (Fig. 6D, E, Supplementary Fig. 5C). Control mice injected with GFP showed no difference in preference index for the zone with the paired odor before or after photostimulation (Fig. 6D, E, Supplementary Fig. 5C).

Together, these results demonstrate that bidirectional manipulation of vGlut2^{BF} neurons elicits opposite effects on learned/associated odor preference. Whereas paired activation of vGlut2^{BF} neurons induces avoidance of odors, inhibition promotes odor preference.

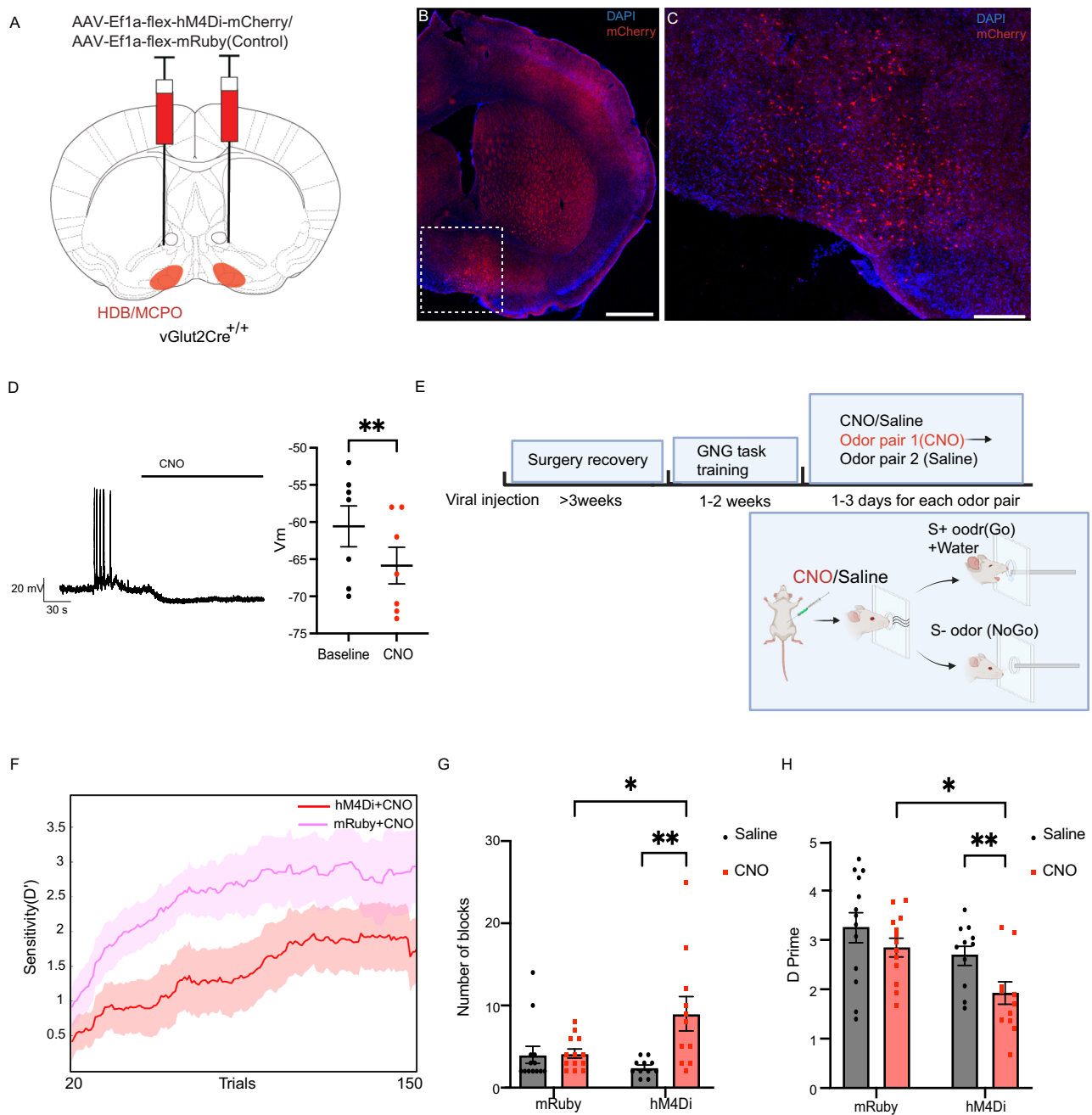
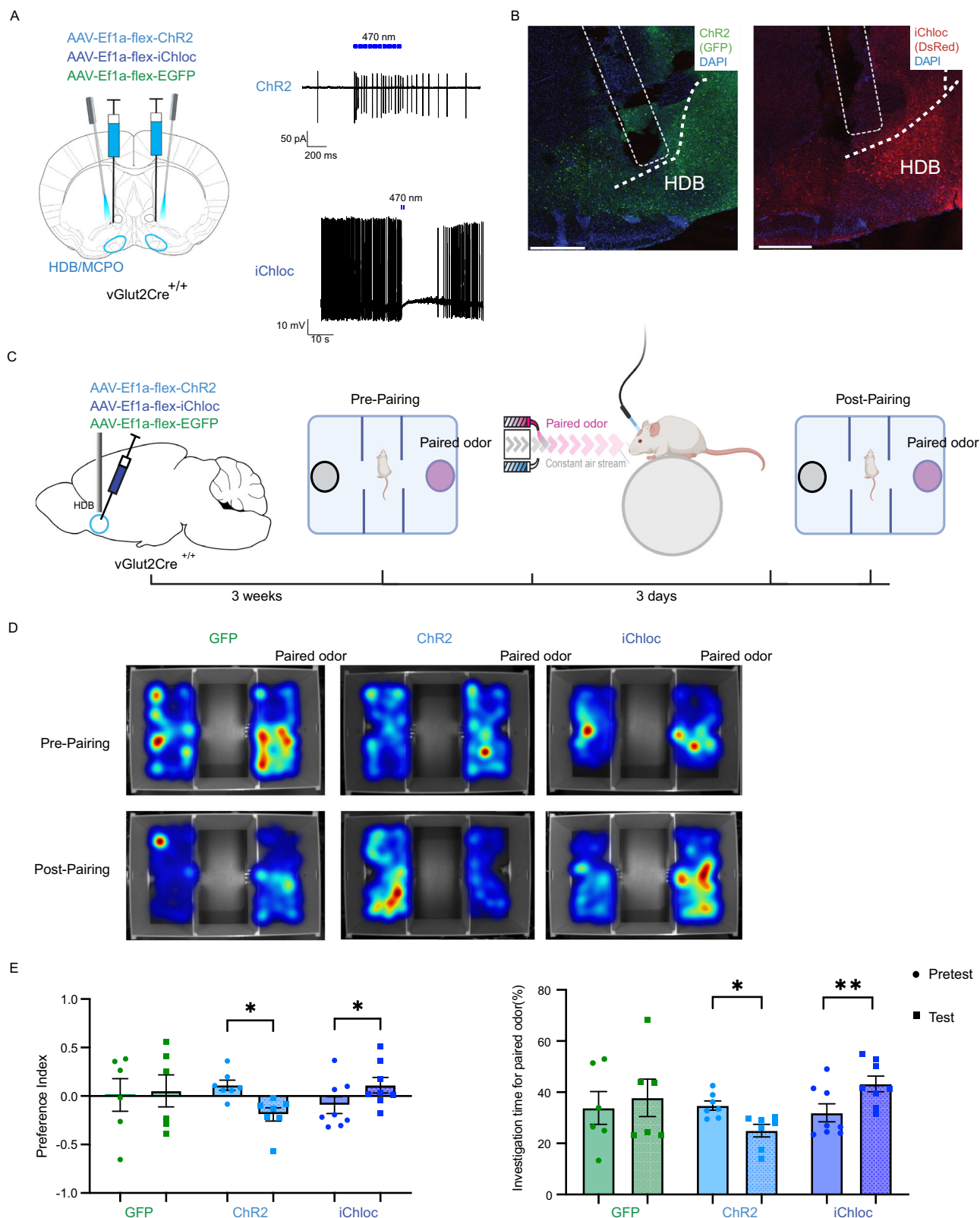


Fig. 5 | vGlut2^{BF} neurons are involved in olfactory learning. **A** Schematic of hM4Di viral injection into vGlut2-expressing basal forebrain (vGlut2^{BF}) neurons for chemogenetic inhibition. **B** Expression of hM4Di-mCherry in glutamatergic neurons of the basal forebrain, highlighting the horizontal limb of the diagonal band (HDB). Scale bar: 500 μ m. **C** Magnified view of mCherry expression in the HDB. Scale bar: 200 μ m. **D** Representative current-clamp recordings from an hM4Di-expressing neuron before and after bath application of CNO (black bar). CNO induced membrane hyperpolarization, quantified as a decrease in membrane potential ($n = 7$ neurons; Paired two-tailed Student's t -test: $p = 0.0028$).

E Experimental paradigm for the olfactory Go/No-Go task. During testing, the S+ odor predicted water reward, whereas the S- odor did not. Each mouse performed two test sessions: one after CNO injection and one after saline injection, using different odor pairs. Mice expressed either hM4Di or a control fluorophore (mRuby). **F** Performance across the testing phase plotted as D-prime (d') using a 40-trial rolling window over 150 trials (starting at trial 20). Each point represents the d'

calculated from a rolling window consisting of the 20 preceding and 20 following trials. Red: hM4Di + CNO; magenta: mRuby + CNO ($n = 11$ hM4Di, $n = 13$ mRuby). **G** Number of 20-trial blocks required to learn each odor pair after saline or CNO. Means \pm s.e.m.: mRuby, 3.22 ± 0.77 ; hM4Di, 6.57 ± 2.42 . Two-way ANOVA with Sidak's multiple comparisons: mRuby (saline vs. CNO), $p = 0.9943$; hM4Di (saline vs. CNO), $p = 0.0022$; saline (mRuby vs. hM4Di), $p = 0.5804$; CNO (mRuby vs. hM4Di), $p = 0.0102$. **H** Maximum d' achieved in each session, calculated from the peak of the 40-trial rolling window. Two-way ANOVA with Sidak's multiple comparisons: mRuby (saline vs. CNO), $p = 0.1074$; hM4Di (saline vs. CNO), $p = 0.083$; saline (mRuby vs. hM4Di), $p = 0.1982$; CNO (mRuby vs. hM4Di), $p = 0.0182$. Data are presented as mean \pm s.e.m. * $P < 0.05$, ** $P < 0.01$. Illustration in (E) was Created in BioRender. Chin, P. (2025) <https://BioRender.com/74qwul9>. Source data are provided as a Source Data file. **A** is reprinted from The Mouse Brain in Stereotaxic Coordinates, 3rd edition, Paxinos G. & Franklin K.B.J., Figures 28, Copyright (2008), with permission from Elsevier.



Discussion

Glutamatergic neurons within the basal forebrain cholinergic nuclei are known to project to subcortical areas involved in both reward and aversion^{16,34–36,61}, positioning them as critical nodes for sensory and behavioral integration via cholinergic signaling. Using in vivo calcium imaging with cellular resolution, we identified a subpopulation of vGlut2^{BF} neurons within cholinergic nuclei that directly respond to a

variety of odors at baseline, including those with distinct innate valences (aversive vs. neutral)^{62,63}. By direct monitoring or using a linear decoder model, we could not differentiate responses to innate aversive or neutral odors under baseline conditions. This is consistent with prior studies showing broad responsivity of vGlut2^{BF} neurons to diverse stimuli^{34–37}. After associative learning, however, vGlut2^{BF} neurons showed increased mean responsivity to conditioned odors, and

Fig. 6 | Activation and inhibition of vGlut2^{BF} neurons alter odor-preference. **A** Schematic of viral injection and optic fiber implantation targeting vGlut2-expressing basal forebrain neurons (vGlut2^{BF}) for optogenetic manipulation (left). Electrophysiological validation of ChR2 and iChloc function (right). Top: cell-attached recordings showing action potentials evoked by 5 ms, 470 nm light pulses in ChR2-expressing neurons. Bottom: reduced firing rate consistent with shunting inhibition in iChloc-expressing neurons during 470 nm illumination. **B** Representative expression patterns of GFP, ChR2, and iChloc in the HDB, along with the fiber track. Scale bar, 500 μ m. **C** Experimental paradigm for the odor preference assay under optogenetic manipulation of vGlut2^{BF} neurons. **D** Representative heat maps of mouse center positions in the behavioral arena. Top: positions prior to pairing the odor with optogenetic manipulation. Bottom:

positions after pairing. From left to right: GFP, ChR2, and iChloc groups. **E** Left: Preference index for the odor-paired region before and after pairing in GFP, ChR2, and iChloc groups. Paired two-tailed Student's *t*-test: GFP ($n = 6$), $p = 0.5802$; ChR2 ($n = 7$), $p = 0.0175$; iChloc ($n = 8$), $p = 0.0104$. Right: Investigation time in the odor-paired region before and after pairing. Paired two-tailed Student's *t*-test: GFP ($n = 6$), $p = 0.3682$; ChR2 ($n = 7$), $p = 0.0200$; iChloc ($n = 8$), $p = 0.0059$. Data are presented as mean \pm s.e.m. * $P < 0.05$, ** $P < 0.01$. Illustrations in (C) was Created in BioRender. Chin, P. (2025) <https://BioRender.com/74qwul9>. Source data are provided as a Source Data file. Left panel in (A) is reprinted from The Mouse Brain in Stereotaxic Coordinates, 3rd edition, Paxinos G. & Franklin K.B.J., Figures 28, Copyright (2008), with permission from Elsevier.

more neurons became responsive. Enhanced decoding accuracy to the odors post-association supports that learning modifies the encoding capacity of this particular neuronal population for conditioned odor stimuli, suggesting a pivotal role in encoding learned sensory information. Additionally, pairing novel odors with appropriately timed vGlut2^{BF} neuronal activity was sufficient to drive positive or negative associations, influencing odor-driven motivational behavior.

Glutamatergic neurons within the BF express nicotinic Acetylcholine (ACh) receptors and receive direct input from cholinergic cells³⁴, suggesting they function downstream of cholinergic signaling. BFCNs show higher activity in response to conditioned sensory cues than non-conditioned cues, with activation occurring immediately after cue presentation^{17,21,64}. Similarly, our results show that vGlut2^{BF} neurons are activated immediately after odor cues, with stronger responses for conditioned odors. This suggests that vGlut2^{BF} neurons may work directly downstream or alongside BFCNs to support sensory-cued associative learning. Previous studies show that in a go/no-go olfactory-cued discrimination task, ACh release in the basal forebrain only increases following reward-associated cues, but not in response to non-rewarding odors⁶⁴. Our findings indicate that vGlut2^{BF} neurons are activated by olfactory stimuli, both with and without associations. Together, these observations may suggest that these neurons may also integrate direct sensory input independent of ACh.

While innate olfactory-driven behaviors are thought to arise from evolutionarily conserved circuits, learned behaviors depend on the selection and reinforcement of neural ensembles throughout an organism's lifetime^{65–67}. For instance, the piriform cortex represents odors and their learned valences, whereas projections from the olfactory bulb to the cortical amygdala mediate innate responses^{62,67–71}. The basal forebrain is connected with both regions^{13,16,34,72}, suggesting its potential role in both innate and learned olfaction-related behaviors. However, our data indicate that while these neurons broadly respond to various odors, they do not differentiate odors with opposite innate valences. Instead, they encode learned odor associations. These findings support previous studies that suggest basal forebrain activity shifts from broad sensory responsiveness to encoding salience during associative learning^{17,21,31,64}.

Our findings show that vGlut2^{BF} neurons encode odors more accurately following positive and/or negative associations. This may suggest that vGlut2^{BF} neurons may share functional similarities with other brain areas like the orbitofrontal cortex⁷⁰ or ventral hippocampus⁷³, both of which enhance encoding capabilities following olfactory associative learning. In fact, these regions may work together to transform sensory information into meaningful representations. Future studies should investigate potential connections between the basal forebrain and the functionally related regions, as well as how these circuits encode learned values over time, adapt during associative learning and extinction, and respond to changes in stimulus values.

In our experimental association paradigm, some initially unresponsive neurons became responsive to odors after associative learning, suggesting that neuronal recruitment may be used to

enhance cortical representations of detected stimuli, facilitating reinforcement-guided behaviors. Previous studies indicate that bursting activity in the basal forebrain is not essential for sensory detection, but that it emerges with learning^{31,74,75}. Further studies exploring the electrophysiology of these newly recruited neurons will be essential for defining the cellular mechanisms by which learning reshapes basal forebrain circuitry.

Our interpretation for why only subsets of vGlut2^{BF} neurons exhibited odor responsiveness is that multiple subtypes exist within this population⁷⁶. For example, McKenna et al. identified subsets of vGlut2^{BF} neurons that co-express calcium-binding protein (Calb) or calcitonin (Calr)⁷⁶. Additionally, vGlut2^{BF} neurons showed diverse responses to odor presentations, which may reflect subset-specific inputs or differential connectivity to downstream targets. Thus, future experiments aimed at identifying molecular markers for these subtypes and further characterizing their anatomies and stimulus-specific responses would be informative. Using such molecular markers could help determine whether specific subtypes are preferentially involved in encoding odor identity versus associative or emotionally salient reinforcement and may further clarify whether the observed heterogeneity in our recordings reflects distinct functional specializations within the vGlut2^{BF} population.

We also noted that most vGlut2^{BF} neurons responded in the same direction to odors with both positive and negative (high-fat diet vs foot shock) associations. Similar response patterns from other BF neurons were proposed to encode associations with primary reinforcement of both valences, suggesting their roles in encoding salience, not valence³¹. However, our model's accuracy in distinguishing between positively and negatively associated odors increased compared to baseline, suggesting that population responses to positively and negatively conditioned odors became more distinct for encoding valences. One previous study showed that cholinergic neurons respond differently to reward vs. punishment. In that study, responses to punishment were more uniform and reliable, independent of stimulus strength, suggesting punishment is always behaviorally unexpected in detection tasks. In contrast, their observed responses to water reward varied with the signal-to-noise ratio of the stimulus. However, these differential responses might also be explained by the difference in reinforcement surprise, representing distinct salient events regardless of valence¹⁷. Since salience represents the importance of the stimulus and refers to the ability to capture attention and facilitate associative learning, foot shock as a punishment and high-fat diet as a reward may be considered much different in their levels of salience⁷⁷. As a result, our observed vGlut2^{BF} neuronal response to these odors may be a composite of multiple features. To further refine this interpretation, additional studies are required to isolate and track each dimension to more clearly decipher what information is being encoded in this population.

Our previous studies showed that overactivation of vGlut2^{BF} drives aversion, while here, we found that inhibition of these neurons can also induce a preference or positive effect. This effect may be mediated by the disinhibition of dopamine release in the Nucleus

accumbens (NAC) through vGlut2^{BF}-to -VTA projections^{36,78}, perhaps creating a positive state. Regardless, together, our data support the idea that vGlut2^{BF} neuronal activity plays a role in modulating motivational behavior.

We have also previously shown that vGlut2^{BF}-to-LHb projections induce a reflexive-like aversion that is not retained as a memory^{35,36}. Specifically, mice failed to learn to avoid a marked side of an arena that was paired with activation of the vGlut2^{BF}-LHb circuit during conditioned place avoidance training. However, our current results show that mice exhibited a reduced preference for an odor paired with vGlut2^{BF} activation, suggesting a learned component in this particular odor-driven behavior. The retention of this negative valence may stem from other inputs involved in sensory processing and/or memory that become stronger and/or better retained with paired stimulation of vGlut2^{BF} cell bodies in the basal forebrain while pairing the stimulation with the odor. This form of paired gain may recruit and/or access additional circuits that generate aversion—such as projections to the VTA and LHb—as well as circuits involved in memory formation, local projections to cholinergic neurons in the BF, or connections to the hippocampus^{13,54,79}. In such a way, the co-activation of these circuits might create a negative experience associated with the odor, leading to altered odor preference.

Since our findings indicate that both positively and negatively associated stimuli increase vGlut2^{BF} neuron responses, the dual role of this population—where activation drives aversion, and inhibition induces preference—may arise from shifts in its homeostatic balance. Artificially altering vGlut2^{BF} activity levels could drive behavioral transitions by disrupting equilibrium, pushing the system toward distinct behavioral states. Future studies should explore the activation thresholds for these opposing effects, focusing on required firing frequencies and/or neuronal recruitment to drive behavioral shifts.

In summary, our study reveals that vGlut2^{BF} neurons respond broadly to olfactory stimuli but do not encode general odor identities. However, following associative learning, they adapt their responses to encode the paired odor stimuli and respond differentially to positive vs. negative associated odor stimuli. Similar to cholinergic neurons and GABAergic neurons within the BF, they contribute to olfactory learning^{32,33,80}. Acute modulation of their activity shifts their associated behaviors to either approach or avoidance, which is consistent with previous studies showing that modulating their projections alters behavior. Notably, we found that this shift in state could be paired with an olfactory stimulus and effectively change its perception. Ultimately, our result demonstrates that vGlut2^{BF} neurons are key contributors to the basal forebrain's role in integrating environmental cues with adaptive behaviors. Since vGlut2^{BF} projections to downstream target brain regions affect a variety of emotionally and/or physiologically salient behaviors, their targeted manipulation may hold potential towards treating related psychiatric disorders such as depression and addiction.

Limitations of the study

Our results demonstrate that vGlut2^{BF} neurons encode odor stimuli more effectively following associative learning. Additionally, our model successfully decodes odors associated with opposing valences. However, it is difficult to balance the strength of positive and negative stimuli precisely. For instance, foot shock, often considered a more salient aversive stimulus, is not directly comparable to a high-fat diet in terms of motivational impact, as reflected in differences in locomotion following odor presentation (see Supplementary Fig. 2I, J). Future studies could use associative paradigms with closely matched reinforcement strengths and sensory modalities to better isolate the underlying valence encoding.

Also worth noting is that our calcium imaging approach lacks the temporal resolution to assess individual action potentials or bursting activity. Future studies using *in vivo* voltage imaging or

electrophysiological recordings of genetically targeted cells are needed to further refine the role of these newly engaged neurons in associative learning⁸¹.

Finally, it remains unclear whether associative learning primarily enhances the system's ability to distinguish odor identities, or if it simply encodes their associated values. To better disentangle these two components, future studies could associate different odors with the same positive or negative stimulus and compare the decoding accuracy within the same value and between the opposite values.

Methods

Animals

All animal care and procedures were approved by Baylor College of Medicine and the licensed BCM IACUC protocol approval committee under protocol number AN5596. All methods have been reported in accordance with recommendations in the ARRIVE guidelines. Mice were maintained on a 12 h light/ 12 h dark cycle with standard chow (Harlan,2920X) and water *ad libitum*. vGlut2-Cre (Slc17a6^{tm2(Cre)Low}/J), Stock No.01696364) mice were purchased from Jackson Laboratories. Male and Female mice were used in all the studies, and no significant sex-specific differences were found. Mice were at least 8 weeks old for stereotaxic surgeries.

Stereotaxic viral injections

Mice were anesthetized and maintained under anesthesia using 1–3% vaporized isoflurane with oxygen. A stereotaxic injection setup was connected to Angle Two software and was used to target the regions of the brain accurately. Viral vectors were delivered through a Nanoliter Injector (NANOJECT II, Drummond Scientific Company) mounted on a stereotaxic platform (Leica Biosystem) at a rate of 23 nL/s. Volumes and coordinates for the viral injections were as follows: Coordinates for all the basal forebrain injections were targeted to anteroposterior (AP) + 0.80 mm, mediolateral (ML) ± 1.00 mm, and dorsoventral (DV) –5.45 mm. For GRIN lens imaging, ~230 nL AAV-hsyn-flex-GCaMP8s (serotype DJ8) was injected on the left side, and the gradient refractive index lens (GRIN lens, diameter, 0.6 mm; length, 7.3 mm, Inscopix) was slowly advanced to 0.1 mm above the basal forebrain and cemented in place with Metabond dental cement (C&B Metabond®) following the viral injection. For the optogenetic manipulation odor-paired experiments, 90–140 nL/sides AAV-Ef1a-flex-Channearhodopsin (serotype DJ8), AAV-Ef1a-flex-iChloc (serotype DJ8), and AAV-Ef1a-flex-GFP (serotype DJ8) were injected, and the optic cannulas [Ø1.25-mm stainless ferrule, Ø200-µm core, 0.22 numerical aperture (NA), 5.33 mm; RWD] were implanted with 5.04 angle and 0.3 mm above the targeted site. For Chemogenetic experiments, AAV-Ef1a-flex-hM4Di (serotype DJ8) and AAV-Ef1a-flex-mRuby2 (serotype DJ8) were injected. All viruses were titered to at least 10¹¹ viral particles/µL. For the following three days of neurosurgery, mice were treated with Meloxicam (Hospira; subcutaneous injection, 5 mg/kg) for pain relief.

Odor presentations

During GRIN lens recordings, mice were head-fixed on a running wheel with a multi-channel olfactometer positioned roughly 7–8 cm in front of their noses. The miniaturized microscope camera (nVoke2; Inscopix Inc.) was placed on the mouse's head during odor presentations. The olfactometer provided a constant stream of room air into which experimental odors were injected. Odors were placed in individual channels, and during each presentation, the selected odor was mixed into the central airstream before being delivered to the mouse through an eductor positioned at the olfactometer output. Arduino-generated TTL pulses triggered the olfactometer and served as digital inputs during recording to precisely align Miniscope imaging data acquired with the nVista Acquisition Software (Inscopix Inc.). The order of odor delivery was controlled by a custom MATLAB program. For odor screening experiments, odorants were delivered for 2 s via injection

into the central air stream with an 18-second interval between deliveries. Odors presented included Rose oil (Rainbow Abby), Eugenol (Sigma 46129), Methyl Salicylate (Sigma M6752), Anisole (Sigma 123226), Butyric acid (Sigma B103500), Cadaverine (Sigma 52063), 2-Methylbutylamine (Sigma 241407), and Isopentylamine (Sigma 126810). For the association experiments, the odors used included Pentanol (Sigma 138975), Hexanol (Sigma H13303), Heptanol (Sigma H2805), and Octanol (Sigma 297887). The odorants were dissolved in mineral oil at 2% concentration for screening and 5% concentration for association experiments by volume and presented in replicates of 10, in a randomized order.

Calcium imaging recording using GRIN lens imaging and imaging processing

Imaging data were acquired using a miniaturized microscope (nVoke2; Inscopix Inc.) after a minimum of 6 weeks post-surgery to ensure sufficient time for surgical recovery, virus expression, and lens image clearing. GCaMP8s signals, indicative of Ca²⁺ activity, were detected using a 435–460 nm excitation LED (1.2 LED power), with a frame rate of 15 FPS. Subsequent analysis of the imaging data was performed using the Inscopix data processing software (IDPS). Videos were pre-processed to correct defective pixels and 4x spatially downsampled. Background fluorescence was removed using a spatial band-pass filter, and fluorescence videos were motion-corrected using the Inscopix motion correction algorithm. We then implemented an independent and principal component analyses (PCA/ICA) algorithm to identify the region of interest, and manually reviewed by the experimenter whether to accept it as a neuron or reject.

Single-neuron analyses for the calcium imaging recordings

Accepted neurons, along with their Ca²⁺ activity traces, were exported to MATLAB for subsequent analysis utilizing custom scripts. To compare neuronal activity between the first exposure and post-association, cells were tracked across sessions using the longitudinal registration function available in the Inscopix Data Processing Software. Z-scored df/f was calculated for the 3 s prior to and 10 s after each odor presentation onset. In conjunction with odor delivery, baseline activity (z-score) was established 2 s before odor onset. Neurons were classified as responsive if their average neuronal activity during odor presentation (2 s) exceeded three standard deviations from the average baseline activity (excited) or their neuronal activity during odor presentation (2 s) was three standard deviations below their baselines (inhibited). The criteria for classifying neurons as excited or inhibited were applied consistently throughout the paper. For all the neurons that are responsive to mineral oil, which served as the solvent of all odors, their activity was baseline-subtracted with their own response to mineral oil. Heat maps and average traces were generated in MATLAB (version 2024).

Olfactory association

Following GRIN lens surgery, mice were subjected to positive and negative association protocols. For negative association, mice were habituated to training chambers for 10 min daily over three days before training. The training involved one session per day for three consecutive days to establish robust odor-shock associations⁸². Each training session comprised five trials, with each trial involving a 10-second odor presentation co-terminating with a 1-second, 0.4-mA foot shock and a 120-second intertrial interval (ITI). The association chambers featured a grid-based floor composed of stainless rods connected to a shock delivery system (ENV-414S, Med Associates). During odor delivery, positive pressure was applied to a reservoir containing 5% Hexanol diluted with mineral oil via a microinjection dispenser (Picospritzer II, Parker).

For positive association, a high-fat diet pellet (#D12492, Research Diets) was introduced into home cages daily for one week,

accompanied by 5% Pentanol dissolved in mineral oil. Mice were fed ad libitum during the association process. This procedure aimed to create a passive association between Pentanol and the high-fat pellets.

For odor habituation, 5% Heptanol was delivered through the olfactometer to the head-fixed mouse for 30 min, with each presentation consisting of 2 s of odor followed by an 18-second inter-trial interval.

Population decoding

We employed multinomial and binary logistic regression models to decode odor identity from neural activity patterns. First, a multinomial logistic regression model was used to discriminate activity patterns among K different odor presentations in one experimental setting:

$$P(y_i = k | X_i) = \frac{\exp(X_i W_k + W_{0,k})}{\sum_{l=0}^{K-1} \exp(X_i W_l + W_{0,l})} \quad (1)$$

where y is the odor presented in trial i to the animal, X_i is a m dimensional vector of the mean activity of m neurons during the 2 s window following odor presentation, W_k is a m dimensional vector of the weights assigned to each neuron, and $W_{0,k}$ is the bias term. The weights are specific to odor k and k set of weights that were estimated in total. The weights and biases of the model were estimated by minimizing the cross-entropy loss with an l-2 regularization. The confusion matrix of the multinomial logistic regression models was visualized to assess the decoding performance.

Subsequently, we implemented binary logistic regression models for pairwise odor discrimination between all combinations of the K odors:

$$p(X_i) = \frac{1}{1 + \exp(-X_i w - w_0)} \quad (2)$$

where $p(X_i)$ the probability of one odor (versus another) being presented in the trial i , X_i is a m dimensional neural activity vector as described above, w the weight vector, and w_0 the bias term. The weights and biases of the model were estimated by minimizing the log loss with an l-2 regularization. To obtain unbiased estimates of decoding performance, we implemented a 5×2 cross-validation procedure. For each fold, trials were randomly partitioned into equal-sized training and test sets. Models were trained on one set and evaluated on the other, and then the sets were swapped, and the process was repeated. This entire procedure was performed five times. The final decoding performance is reported as the mean accuracy across all test sets.

Odor preference tests

A custom-designed three-chamber box, created by the engineering core at Baylor College of Medicine, was used for behavioral tests. The experiments were set up as “pretest” (before odor pairing) and “test” (after odor pairing). During both pretest and test, mice were placed in the chamber for 10 min to habituate to the environment and the tea diffusers. Following habituation, tea diffusers containing 100 μ L of 5% odor solution in mineral oil on gauze were placed at the center edge of each side chamber. Each mouse ran 10 min for the preference test. EthoVision XT software (XT 16; <https://www.noldus.com/ethovision-xt>) was used to track the time the mice spent in each region.

For the odor pairing experiment, the preference index was defined as the time spent in the paired odor zone minus the time spent in the unpaired odor zone divided by the total time spent in both zones. We then compared the preference index for the paired odor before odor pairing with that after. The mice had a preference for the paired odor during pretest, defined as spending more than 75% of time in the paired odor side were excluded from the analysis.

In vitro electrophysiology

For acute basal forebrain slice preparation, animals were anesthetized with isoflurane and perfused with a cold artificial cerebrospinal fluid (ACSF) solution containing 125 mM NaCl, 2.5 mM KCl, 1.25 mM NaH₂PO₄, 2 mM CaCl₂, 1 mM MgCl₂, 10 mM glucose, and 25 mM NaHCO₃. Brains were removed and transferred into an ice-cold cutting solution (pH 7.35) containing 87 mM NaCl, 2.5 mM KCl, 1.25 mM NaH₂PO₄, 0.5 mM CaCl₂, 7 mM MgCl₂·6H₂O, 13 mM ascorbic acid, 75 mM sucrose, 10 mM glucose, and 25 mM NaHCO₃. Both solutions were pH-equilibrated with a 5% CO₂/95% O₂ gas mixture for at least 10 minutes before the experiment. 300 micrometer thick coronal forebrain slices were prepared using a Leica VT1200 vibratome and placed at least 15 min at 37 °C in 5% CO₂/95% O₂ bubbled ACSF solution. They were then gradually lowered to ambient temperature (25 °C) and allowed to acclimate for at least 15 minutes before recording.

For recording, slices were transferred into a recording chamber perfused with ACSF at 1.5–2 mL/min at 25 °C. Neurons were identified by an optiMOS camera (QImaging) controlled by Micro-Manager version 1.4.22 software (University of California at San Francisco) using 900 nm DIC (Olympus BX50WI) optics, and fluorescence reporter using Thorlabs DC4100 470-nm or 565-nm LED illumination with 49002-ET-EGFP (FITC/Cy2) or HcRed1 emission filters (Chroma Technology), respectively. Recordings were acquired using an Axon MultiClamp 700B amplifier digitized at 10 kHz (Axon Digidata 1440 A). Recording electrodes (3–5 MΩ) were fabricated from borosilicate glass microcapillaries (outer diameter 1.5 mm) with a micropipette puller (Sutter Instruments). The internal solution contained 110 mM K-gluconate, 10 mM KCl, 4 mM ATP-Mg, 0.5 mM GTP-Na, 10 mM phosphocreatine-di-Na, 1 mM EGTA, 10 mM HEPES; pH was adjusted to 7.3 with KOH, and the osmolarity was adjusted to 305 mOsm/L with K-gluconate. The access resistance was monitored throughout the experiment and was typically in a range of 10–20 MΩ and considered acceptable up to 30 MΩ. Obtained recordings were processed offline using Clampfit 10.7.0.3 (Molecular Devices).

In total, 22 BF neurons from 8 animals were recorded. Of those, 7 didn't show spontaneous AP activity, while others demonstrated irregular firing activity at 6.05 ± 1.78 Hz. To test the inhibitory response of the hM4Di receptor, neurons were recorded in current clamp mode to measure baseline firing and voltage changes before and after CNO bath application. To test the optogenetic tools for controlling neuronal activity, cells were recorded in either cell-attached or whole-cell current clamp mode. The ChR2-induced firing was evoked by 20 Hz, 5 ms, 470 nm light pulses. For iChloc validation, cells were monitored for changes in membrane voltage and firing frequency (spontaneous or slow current induced) for 30 s before and 30 s after 470 nm light pulses at 1 Hz, 2 s.

Go/no-go training

Freely moving mice underwent training in an olfactory-based go/no-go discrimination task utilizing olfactory association chambers manufactured by Med Associates and controlled by MedPC software. These chambers featured a designated odor delivery port and a water port, each with infrared beams to track entries. The odor delivery port maintained a consistent flow of purified room air, facilitated by a vacuum system. These chambers were situated within larger behavioral isolation boxes, also provided by Med Associates. Within these boxes, box fans operated continuously to facilitate ambient air circulation away from the association chambers, mitigating the buildup of ambient odors.

Odors were introduced into the continuous airflow by activating valves connected to one of two odor reservoirs. This enabled the airflow to pass through the headspace of the reservoir containing the volatilized odor. These reservoirs, each 20 mL in volume, contained 2.5 mL of odor diluted to a 1% concentration in mineral oil. Water

rewards, dispensed in volumes of 5 μL, were provided exclusively in the distinct reward port upon successfully completing “Hit” trials.

Mice underwent five stages of training to learn to perform the Go/No-Go task as previously described⁶⁴ for 10–14 days. Mice were first water-restricted to no less than 85 % of their body weight. They were then trained to associate an S+ odor cue (1% Eugenol in mineral oil) with receiving a water reward. After this association was successfully formed, an S-odor cue (1% Methyl Salicylate in mineral oil) was introduced. During this phase, mice were trained to avoid seeking a reward when presented with the S-odor and instead initiate a new trial; otherwise, they would receive a 4-second time-out punishment. This training phase was considered complete once the mice achieved over 85% accuracy in at least two consecutive blocks of trials. After they learned to go for the S+ odor for reward and not to go for the S- odor, they were moved to the testing phase. In the testing sessions, the same procedure was followed, but new odor pairs were introduced in each session. For saline treatment, the odor pair was Isoamyl acetate (Sigma w205508) and 2-heptanone (Sigma 02476); for CNO treatment, the odor pair was Alpha-pinene (Sigma 147524) and 2-Methylpyrazine (Sigma M75608).

Performance in the go/no-go task was assessed using signal detection theory, specifically the d' ($d' = Z(\text{Hit Rate}) - Z(\text{False Alarm Rate})$), which quantifies sensitivity and overall task performance. The hit rate was defined as the proportion of trials in which the mouse correctly sought a water reward within 5 s of S+ odor presentation, and the false alarm rate as the proportion of trials in which the mouse incorrectly attempted to retrieve water during S- odor presentation. Both rates were converted to z-scores using the inverse cumulative distribution function of the standard normal distribution, and d' was computed as their difference. To evaluate changes in sensitivity over time within a session, d' was computed using a rolling window of 40 trials. The session summary d' values were determined as the maximum d' within this rolling window, excluding early trials where mice were learning new S+ and S- associations and later trials where task engagement may have declined. The overall performance was calculated using the Hit rate and the False alarm rate across the whole test. Learning ability was assessed by calculating the number of blocks (each consisting of 20 trials) required to first meet the criterion of 85% correct trials. Summary d' calculations and rolling-window plots across trials were generated using custom MATLAB scripts.

Odor discrimination

Spontaneous odor discrimination was evaluated using a habituation/dishabituation assay^{83,84}. Mice were initially habituated to the test chamber, which contained blank tea diffusers, for 10 minutes before the experiment began. Following habituation, removable walls were placed to divide the chamber into three compartments, restricting the mouse to the central compartment. Tea diffusers containing 50 μL of 2% odor in mineral oil on gauze were positioned at the center of each side chamber's edge. At the start of the experiment, the dividers were removed, and the time the mice spent near the tea diffusers was recorded.

Every 2 minutes, the removable walls were reinserted, and the gauzes with the odors in the tea diffusers were renewed. After renewing the odors, the walls were removed again, initiating the subsequent 2-minute trial. During the first three trials (Habituation phase), both tea diffusers contained the same odor: Acetophenone (Sigma A10701) for the CNO group and Isoamyl acetate (Sigma W205508) for the Saline group. During the fourth trial (Dishabituation phase), one tea diffuser contained the initial odor (odor1), and the other diffuser contained a new odor (odor2): Anisole (Sigma 123226) for the CNO group and isoamyl butyrate (W206008 Sigma) for the saline group. Behavioral data were captured using a Noldus behavior tracking camera, and EthoVision XT software (XT 16; <https://www.noldus.com/>)

ethovision-xt) was used to track the time spent by the mice in each compartment.

Real-time place preference/ avoidance (RTPP/RTPA)

We used a Noldus Phentoper divided into two halves for these experiments: one paired with photostimulation and the other without. Mice were placed in the chamber for three days to habituate, during which baseline tracking data were collected using EthoVision XT software (XT 16; <https://www.noldus.com/ethovision-xt>). After the habituation period, mice were tracked in the chamber for 30 minutes, with a light pulse applied whenever they entered the photostimulation-paired side. We compared the time spent on the photostimulation-paired side during the experiment to the baseline time spent on the same side during habituation.

Odor-light pairing

Before pairing, mice were placed in a three-chamber setting for 10 minutes to evaluate their preference for two odors (5% Pentanol and 5% Hexanol v/v in mineral oil). The odors were contained within tea filters, with one positioned on the left side and the other on the right side of the chamber. During pairing, the mice were first head-fixed and habituated on the running wheel each pairing day for 15 minutes. Pentanol and Hexanol were randomly delivered to the mice using an olfactometer⁵⁰ with a delivery duration of 2 s and a 30-second inter-stimulus interval. Each session consisted of 20 trials, repeated for 5 sessions. During pairing, only Hexanol was simultaneously delivered with 2-second, 20 Hz trains of light pulses (10 ms, 473 nm) for targeted neuronal activation in CHR2-expressing mice. The same pairing paradigm was used in GFP-expressing mice as controls. Conversely, only Pentanol was simultaneously delivered with 2-second, 0.5 Hz trains of light pulses (10 ms, 473 nm) for neuronal inhibition in iChloc-expressing mice. Following three days of odor pairing, mice were reassessed in the same three-chamber setting to evaluate their preference for the odors.

Post-hoc analysis

Perfusion and tissue dissection. Animals were transcardially perfused with PBS, followed by 4% paraformaldehyde (PFA) perfusion. Brains were then post-fixed in 4% PFA solution at 4 °C for at least one day, followed by overnight cryoprotection in 30% sucrose. Cryoprotected brains were subsequently embedded and frozen in O.C.T. (Fisher HealthCare No. 4585) and stored at -80 °C until sectioning. Coronal sections measuring 40-50 μm thick were obtained using a cryostat (Leica CM1860), with every third section collected. The slices for checking the targeting for optogenetics, chemogenetics, and GRIN lens experiments were then mounted onto microscope slides with DAPI Fluoromount-G (Southern Biotech, 0100-20), and images were acquired using a Leica SP8X confocal microscope.

Quantification and Statistical Analysis. GraphPad Prism 10.2.0 (GraphPad Software, Inc., La Jolla, CA, USA) was used for all statistical analyses and figure generation. Figures illustrating mean response, heat maps, and PCA trajectories for the calcium imaging data were generated using MATLAB scripts.

The Euclidean distance measures how different the activity patterns of the neuronal population are when responding to different stimuli. Specifically, we created a vector representing the mean population response to each odor, with each element corresponding to the activity of an individual neuron. We then calculated the Euclidean distance between these vectors, which quantifies the overall dissimilarity between the two response patterns. Larger distances indicate more distinct representations of the odors across the recorded neurons. To calculate the Euclidean distance between neural activity vectors derived from calcium imaging data, the neural activity matrix was first reduced to mean activity vectors by averaging across

trials. The Euclidean distance between these vectors was computed using the formula

$$\sqrt{\sum_{k=1}^n (A_{\text{exp}} - A_{\text{control}})^2} \quad (3)$$

where n represents the number of neurons, A_{exp} and A_{control} represent the average neuronal activity under the experimental and the control odors.

The trial reliability of neural responses to odor presentations was assessed by calculating correlations between subsets of trials. Specifically, all trials were randomly divided into two halves, and the correlation between the average neural activity of each half was computed. This procedure was repeated 10 times, and the final trial reliability value was obtained by averaging the correlations across all 10 iterations.

Statistical analyses were performed to assess differences across conditions. Paired two-tailed Student's *t*-tests were used to compare the time spent in the conditioned odor zone versus the mineral oil zone. They were also applied to evaluate changes in mean neuronal responses before and after association across odor groups, the accuracy of the binary classifier for different odors, and the Euclidean distance both before and after association, as well as between odors. Finally, paired two-tailed Student's *t*-tests were used to compare the preference index for the paired odor and the time spent in each zone before and after odor pairing across manipulations.

To assess reliability across different odors and associations and the number of trials required for learning the Go/No-Go task, we conducted a two-way repeated measures ANOVA followed by Sidak's multiple comparisons. The same analysis was used to compare *d*-prime values for Go/No-Go task performance across treatments and mouse groups, and the time spent in the region with paired odors across different mouse groups and time points.

For odor discrimination tasks, a one-sample *t*-test was used to determine whether preference for a novel odor significantly differed from zero. Throughout all experiments, statistical significance was defined as $p < 0.05$. Detailed statistical information, including exact sample sizes and representations for each experiment, is provided in the text and figure legend.

Reporting summary

Further information on research design is available in the Nature Portfolio Reporting Summary linked to this article.

Data availability

Source data are provided with this paper. Additional datasets not included in the source-data Excel file are available at Zenodo: <https://doi.org/10.5281/zenodo.17704682> Source data are provided with this paper.

Code availability

All original code has been deposited at Github https://github.com/julie200388/vGlut2BF_odor_learning.

References

- Gilbert, C. D. & Sigman, M. Brain states: top-down influences in sensory processing. *Neuron* **54**, 677–696 (2007).
- Chun, M. M., Golomb, J. D. & Turk-Browne, N. B. A taxonomy of external and internal attention. *Annu. Rev. Psychol.* **62**, 73–101 (2011).
- Ananth, M. R., Rajebhosale, P., Kim, R., Talmage, D. A. & Role, L. W. Basal forebrain cholinergic signalling: development, connectivity and roles in cognition. *Nat. Rev. Neurosci.* **24**, 233–251 (2023).

4. Ballinger, E. C., Ananth, M., Talmage, D. A. & Role, L. W. Basal forebrain cholinergic circuits and signaling in cognition and cognitive decline. *Neuron* **91**, 1199–1218 (2016).
5. Nunez-Parra, A., Maurer, R. K., Krahe, K., Smith, R. S. & Araneda, R. C. Disruption of centrifugal inhibition to olfactory bulb granule cells impairs olfactory discrimination. *Proc. Natl. Acad. Sci. USA* **110**, 14777–14782 (2013).
6. Gritton, H. J. et al. Cortical cholinergic signaling controls the detection of cues. *Proc. Natl. Acad. Sci. USA* **113**, E1089–E1097 (2016).
7. Pinto, L. et al. Fast modulation of visual perception by basal forebrain cholinergic neurons. *Nat. Neurosci.* **16**, 1857–1863 (2013).
8. Goard, M. & Dan, Y. Basal forebrain activation enhances cortical coding of natural scenes. *Nat. Neurosci.* **12**, 1444–1449 (2009).
9. Meir, I., Katz, Y. & Lampl, I. Membrane potential correlates of network decorrelation and improved SNR by cholinergic activation in the somatosensory cortex. *J. Neurosci.* **38**, 10692–10708 (2018).
10. Mincses, V., Pinto, L., Dan, Y. & Chiba, A. A. Cholinergic shaping of neural correlations. *Proc. Natl. Acad. Sci. USA* **114**, 5725–5730 (2017).
11. Zhu, F., Elnozahy, S., Lawlor, J. & Kuchibhotla, K. V. The cholinergic basal forebrain provides a parallel channel for state-dependent sensory signaling to auditory cortex. *Nat. Neurosci.* **26**, 810–819 (2023).
12. Chaudhury, D., Escanilla, O. & Linster, C. Bulbar acetylcholine enhances neural and perceptual odor discrimination. *J. Neurosci.* **29**, 52–60 (2009).
13. Hu, R., Jin, S., He, X., Xu, F. & Hu, J. Whole-Brain Monosynaptic Afferent Inputs to Basal Forebrain Cholinergic System. *Front. Neuroanat.* **10**, 98 (2016).
14. Xu, M. et al. Basal forebrain circuit for sleep-wake control. *Nat. Neurosci.* **18**, 1641–1647 (2015).
15. Gielow, M. R. & Zaborszky, L. The Input-Output Relationship of the Cholinergic Basal Forebrain. *Cell Rep.* **18**, 1817–1830 (2017).
16. Do, J. P. et al. Cell type-specific long-range connections of basal forebrain circuit. *eLife* **5**, e13214 (2016).
17. Hangya, B., Ranade, S. P., Lorenc, M. & Kepecs, A. Central cholinergic neurons are rapidly recruited by reinforcement feedback. *Cell* **162**, 1155–1168 (2015).
18. Harrison, T. C., Pinto, L., Brock, J. R. & Dan, Y. Calcium Imaging of Basal Forebrain Activity during Innate and Learned Behaviors. *Front. Neural Circuits* **10**, 36 (2016).
19. Robert, B. et al. A functional topography within the cholinergic basal forebrain for encoding sensory cues and behavioral reinforcement outcomes. *eLife* **10**, e69514 (2021).
20. Rajebhosale, P. et al. Functionally refined encoding of threat memory by distinct populations of basal forebrain cholinergic projection neurons. *eLife* **13**, e86581 (2024).
21. Hegedüs, P., Sviatkó, K., Király, B., Martínez-Bellver, S. & Hangya, B. Cholinergic activity reflects reward expectations and predicts behavioral responses. *iScience* **26**, 105814 (2023).
22. Stephenson-Jones, M. et al. Opposing contributions of gabaergic and glutamatergic ventral pallidal neurons to motivational behaviors. *Neuron* **105**, 921–933.e5 (2020).
23. Kim, R., Ananth, M. R., Desai, N. S., Role, L. W. & Talmage, D. A. Distinct subpopulations of ventral pallidal cholinergic projection neurons encode valence of olfactory stimuli. *Cell Rep.* **43**, 114009 (2024).
24. Gritti, I., Mainville, L., Mancina, M. & Jones, B. E. GABAergic and other noncholinergic basal forebrain neurons, together with cholinergic neurons, project to the mesocortex and isocortex in the rat. *J. Comp. Neurol.* **383**, 163–177 (1997).
25. Tingley, D., Alexander, A. S., Quinn, L. K., Chiba, A. A. & Nitz, D. A. Cell assemblies of the basal forebrain. *J. Neurosci.* **35**, 2992–3000 (2015).
26. Gritti, I. et al. Stereological estimates of the basal forebrain cell population in the rat, including neurons containing choline acetyltransferase, glutamic acid decarboxylase or phosphate-activated glutaminase and colocalizing vesicular glutamate transporters. *Neuroscience* **143**, 1051–1064 (2006).
27. Zou, Y. et al. Cell-type-specific optogenetic fMRI on basal forebrain reveals functional network basis of behavioral preference. *Neuron* **112**, 1342–1357.e6 (2024).
28. Yang, C., Thankachan, S., McCarley, R. W. & Brown, R. E. The menagerie of the basal forebrain: how many (neural) species are there, what do they look like, how do they behave and who talks to whom?. *Curr. Opin. Neurobiol.* **44**, 159–166 (2017).
29. Yang, C. et al. Cholinergic neurons excite cortically projecting basal forebrain GABAergic neurons. *J. Neurosci.* **34**, 2832–2844 (2014).
30. Henny, P. & Jones, B. E. Projections from basal forebrain to prefrontal cortex comprise cholinergic, GABAergic and glutamatergic inputs to pyramidal cells or interneurons. *Eur. J. Neurosci.* **27**, 654–670 (2008).
31. Lin, S.-C. & Nicolelis, M. A. L. Neuronal ensemble bursting in the basal forebrain encodes salience irrespective of valence. *Neuron* **59**, 138–149 (2008).
32. Zhou, P., Liu, P., Zhang, Y., Wang, D. & Li, A. The response dynamics and function of cholinergic and gabaergic neurons in the basal forebrain during olfactory learning. *Front. Cell. Neurosci.* **16**, 911439 (2022).
33. Moss, E. H. et al. Distinct Patterns of PV and SST GABAergic Neuronal Activity in the Basal Forebrain during Olfactory-Guided Behavior in Mice. *J. Neurosci.* **45**, e0200242025 (2025).
34. Patel, J. M. et al. Sensory perception drives food avoidance through excitatory basal forebrain circuits. *eLife* **8**, e44548 (2019).
35. Swanson, J. L. et al. Activation of basal forebrain-to-lateral habenula circuitry drives reflexive aversion and suppresses feeding behavior. *Sci. Rep.* **12**, 22044 (2022).
36. Cai, J. et al. An excitatory projection from the basal forebrain to the ventral tegmental area that underlies anorexia-like phenotypes. *Neuron* **112**, 458–472.e6 (2024).
37. Cai, P. et al. A glutamatergic basal forebrain to midbrain circuit mediates wakefulness and defensive behavior. *Neuropharmacology* **208**, 108979 (2022).
38. Fu, Y. The dual action of basal forebrain in feeding regulation. *Nat. Metab.* (2024) <https://doi.org/10.1038/s42255-024-01111-x>.
39. Golden, S. A. et al. Basal forebrain projections to the lateral habenula modulate aggression reward. *Nature* **534**, 688–692 (2016).
40. Wang, J. et al. The basal forebrain to lateral habenula circuitry mediates social behavioral maladaptation. *Nat. Commun.* **15**, 4013 (2024).
41. Peng, W. et al. Regulation of sleep homeostasis mediator adenosine by basal forebrain glutamatergic neurons. *Science* **369**, eabb0556 (2020).
42. Zheng, Y. et al. Different subgroups of cholinergic neurons in the basal forebrain are distinctly innervated by the olfactory regions and activated differentially in olfactory memory retrieval. *Front. Neural Circuits* **12**, 99 (2018).
43. Li, X. et al. Generation of a whole-brain atlas for the cholinergic system and mesoscopic projectome analysis of basal forebrain cholinergic neurons. *Proc. Natl. Acad. Sci. USA* **115**, 415–420 (2018).
44. Rye, D. B., Wainer, B. H., Mesulam, M. M., Mufson, E. J. & Saper, C. B. Cortical projections arising from the basal forebrain: a study of cholinergic and noncholinergic components employing combined retrograde tracing and immunohistochemical localization of choline acetyltransferase. *Neuroscience* **13**, 627–643 (1984).
45. Niedworok, C. J. et al. Charting monosynaptic connectivity maps by two-color light-sheet fluorescence microscopy. *Cell Rep.* **2**, 1375–1386 (2012).

46. Gracia-Llanes, F. J. et al. GABAergic basal forebrain afferents innervate selectively GABAergic targets in the main olfactory bulb. *Neuroscience* **170**, 913–922 (2010).
47. Záborszky, L., Carlsen, J., Brashear, H. R. & Heimer, L. Cholinergic and GABAergic afferents to the olfactory bulb in the rat with special emphasis on the projection neurons in the nucleus of the horizontal limb of the diagonal band. *J. Comp. Neurol.* **243**, 488–509 (1986).
48. Smith, R. S. et al. Differential muscarinic modulation in the olfactory bulb. *J. Neurosci.* **35**, 10773–10785 (2015).
49. Paolini, A. G. & McKenzie, J. S. Effects of lesions in the horizontal diagonal band nucleus on olfactory habituation in the rat. *Neuroscience* **57**, 717–724 (1993).
50. Burton, S. D., Wipfel, M., Guo, M., Eiting, T. P. & Wachowiak, M. A novel olfactometer for efficient and flexible odorant delivery. *Chem. Senses* **44**, 173–188 (2019).
51. Saraiva, L. R. et al. Combinatorial effects of odorants on mouse behavior. *Proc. Natl. Acad. Sci. USA* **113**, E3300–E3306 (2016).
52. Li, Q. & Liberles, S. D. Aversion and attraction through olfaction. *Curr. Biol.* **25**, R120–R129 (2015).
53. Dewan, A., Pacifico, R., Zhan, R., Rinberg, D. & Bozza, T. Non-redundant coding of aversive odours in the main olfactory pathway. *Nature* **497**, 486–489 (2013).
54. Zheng, Y. et al. Basal Forebrain-Dorsal Hippocampus Cholinergic Circuit Regulates Olfactory Associative Learning. *Int. J. Mol. Sci.* **23**, 8472 (2022).
55. Neyhart, E. et al. Cortical acetylcholine dynamics are predicted by cholinergic axon activity and behavior state. *Cell Rep.* **43**, 114808 (2024).
56. Yang, C., McKenna, J. T. & Brown, R. E. Intrinsic membrane properties and cholinergic modulation of mouse basal forebrain glutamatergic neurons in vitro. *Neuroscience* **352**, 249–261 (2017).
57. Liu, G. et al. An objective and reproducible test of olfactory learning and discrimination in mice. *J. Vis. Exp.* (2018) <https://doi.org/10.37971/57142>.
58. Stanislaw, H. & Todorov, N. Calculation of signal detection theory measures. *Behav. Res. Methods Instrum. Comput.* **31**, 137–149 (1999).
59. Messier, J. E., Chen, H., Cai, Z.-L. & Xue, M. Targeting light-gated chloride channels to neuronal somatodendritic domain reduces their excitatory effect in the axon. *eLife* **7**, e38506 (2018).
60. Wietek, J. et al. An improved chloride-conducting channelrhodopsin for light-induced inhibition of neuronal activity in vivo. *Sci. Rep.* **5**, 14807 (2015).
61. Hur, E. E. & Zaborszky, L. Vglut2 afferents to the medial prefrontal and primary somatosensory cortices: a combined retrograde tracing in situ hybridization study [corrected]. *J. Comp. Neurol.* **483**, 351–373 (2005).
62. Root, C. M., Denny, C. A., Hen, R. & Axel, R. The participation of cortical amygdala in innate, odour-driven behaviour. *Nature* **515**, 269–273 (2014).
63. Iurilli, G. & Datta, S. R. Population coding in an innately relevant olfactory area. *Neuron* **93**, 1180–1197.e7 (2017).
64. Hanson, E., Brandel-Ankrapp, K. L. & Arenkiel, B. R. Dynamic Cholinergic Tone in the Basal Forebrain Reflects Reward-Seeking and Reinforcement During Olfactory Behavior. *Front. Cell. Neurosci.* **15**, 635837 (2021).
65. Choi, G. B. et al. Driving opposing behaviors with ensembles of piriform neurons. *Cell* **146**, 1004–1015 (2011).
66. Kobayakawa, K. et al. Innate versus learned odour processing in the mouse olfactory bulb. *Nature* **450**, 503–508 (2007).
67. Stettler, D. D. & Axel, R. Representations of odor in the piriform cortex. *Neuron* **63**, 854–864 (2009).
68. Miyamichi, K. et al. Cortical representations of olfactory input by trans-synaptic tracing. *Nature* **472**, 191–196 (2011).
69. Ghosh, S. et al. Sensory maps in the olfactory cortex defined by long-range viral tracing of single neurons. *Nature* **472**, 217–220 (2011).
70. Wang, P. Y. et al. Transient and persistent representations of odor value in prefrontal cortex. *Neuron* **108**, 209–224.e6 (2020).
71. Sosulski, D. L., Bloom, M. L., Cutforth, T., Axel, R. & Datta, S. R. Distinct representations of olfactory information in different cortical centres. *Nature* **472**, 213–216 (2011).
72. Ortiz-Guzman, J. et al. Cholinergic basal forebrain connectivity to the basolateral amygdala modulates food intake. *eNeuro* **11**, ENEURO.0369–23.2024 (2024).
73. Biane, J. S. et al. Neural dynamics underlying associative learning in the dorsal and ventral hippocampus. *Nat. Neurosci.* **26**, 798–809 (2023).
74. Lin, S.-C., Brown, R. E., Hussain Shuler, M. G., Petersen, C. C. H. & Kepecs, A. Optogenetic dissection of the basal forebrain neuromodulatory control of cortical activation, plasticity, and cognition. *J. Neurosci.* **35**, 13896–13903 (2015).
75. Avila, I. & Lin, S.-C. Motivational salience signal in the basal forebrain is coupled with faster and more precise decision speed. *PLoS Biol.* **12**, e1001811 (2014).
76. McKenna, J. T. et al. Characterization of basal forebrain glutamate neurons suggests a role in control of arousal and avoidance behavior. *Brain Struct. Funct.* **226**, 1755–1778 (2021).
77. Pearce, J. M. & Hall, G. A model for Pavlovian learning: variations in the effectiveness of conditioned but not of unconditioned stimuli. *Psychol. Rev.* **87**, 532–552 (1980).
78. Qi, J. et al. VTA glutamatergic inputs to nucleus accumbens drive aversion by acting on GABAergic interneurons. *Nat. Neurosci.* **19**, 725–733 (2016).
79. Wu, H., Williams, J. & Nathans, J. Complete morphologies of basal forebrain cholinergic neurons in the mouse. *eLife* **3**, e02444 (2014).
80. Nunez-Parra, A., Cea-Del Rio, C. A., Huntsman, M. M. & Restrepo, D. The basal forebrain modulates neuronal response in an active olfactory discrimination task. *Front. Cell. Neurosci.* **14**, 141 (2020).
81. Zhou, Z. C. et al. Deep-brain optical recording of neural dynamics during behavior. *Neuron* **111**, 3716–3738 (2023).
82. Morrison, F. G., Dias, B. G. & Ressler, K. J. Extinction reverses olfactory fear-conditioned increases in neuron number and glomerular size. *Proc. Natl. Acad. Sci. USA* **112**, 12846–12851 (2015).
83. Papes, F., Nakahara, T. S. & Camargo, A. P. Behavioral assays in the study of olfaction: A practical guide. *Methods Mol. Biol.* **1820**, 289–388 (2018).
84. Lyons-Warren, A. M. et al. Co-transmitting interneurons in the mouse olfactory bulb regulate olfactory detection and discrimination. *Cell Rep.* **42**, 113471 (2023).

Acknowledgements

Special thanks to the Neurological Research Institute Viral Core (including Zihong Chen and Ying Wang) for production of AAVs used in these experiments. Additionally, thanks to members of the Arenkiel lab for their collaboration and help in editing this manuscript. We thank Inscopix field scientists Dr. Waylin Yu, Dr. Jing Liang-Guallpa, and Dr. Matthew Whitmire for their technical support with GRIN lens microscope imaging. We also appreciate Dr. Elizabeth H. Moss, Dr. Matthew J. McGinley, Dr. Ariel Lyons-Warren, and Snigdha Srivastava for their valuable conceptual input during the writing of this manuscript. This work was supported by DoD award PR22135 to BRA and QT, R01DK109934 to BRA and QT, R01DK138518 to BRA, USDA project # 58-3092-5-008 to BRA, and P50HD103555.

Author contributions

P.C.: conceptualization, experimental design, conducting experiments, collecting data, data analysis, manuscript writing and editing, and figure creation. Z.D.: experimental design, data analysis, manuscript writing.

M.Y.K.: data collection, data analysis, figure creation, manuscript writing. S.S.: data collection. E.H.M.: data analysis, manuscript editing. Q.T.: conceptualization, mentorship, manuscript editing. B.R.A.: mentorship, conceptualization, experimental design, data analysis, and manuscript editing.

Competing interests

The authors declare no competing interests.

Additional information

Supplementary information The online version contains supplementary material available at <https://doi.org/10.1038/s41467-026-68313-7>.

Correspondence and requests for materials should be addressed to Qingchun Tong or Benjamin R. Arenkiel.

Peer review information *Nature Communications* thanks Min Xu and the other anonymous reviewer(s) for their contribution to the peer review of this work. A peer review file is available.

Reprints and permissions information is available at <http://www.nature.com/reprints>

Publisher's note Springer Nature remains neutral with regard to jurisdictional claims in published maps and institutional affiliations.

Open Access This article is licensed under a Creative Commons Attribution-NonCommercial-NoDerivatives 4.0 International License, which permits any non-commercial use, sharing, distribution and reproduction in any medium or format, as long as you give appropriate credit to the original author(s) and the source, provide a link to the Creative Commons licence, and indicate if you modified the licensed material. You do not have permission under this licence to share adapted material derived from this article or parts of it. The images or other third party material in this article are included in the article's Creative Commons licence, unless indicated otherwise in a credit line to the material. If material is not included in the article's Creative Commons licence and your intended use is not permitted by statutory regulation or exceeds the permitted use, you will need to obtain permission directly from the copyright holder. To view a copy of this licence, visit <http://creativecommons.org/licenses/by-nc-nd/4.0/>.

© The Author(s) 2026